FEATURE ARTICLE

Electronic Structure and Bonding in Actinyl Ions and their Analogs

Robert G. Denning†

Inorganic Chemistry Laboratory, University of Oxford, South Parks Road, Oxford OX1 3QR, United Kingdom

Received: February 7, 2007

This Feature Article seeks to present the current state of knowledge, both experimental and theoretical, of the electronic structure and bonding in actinyl ions and related species, such as the isoelectronic imido compounds as well as in linear triatomic actinide molecules of the type X−An−Y.

I. Introduction

In the actinyl ions, AnO_2^{n+}, the actinide−oxygen bonds are short, strong, and collinear; these are chemically robust species. For example, the mean U−O bond enthalpy for dissociation to oxygen atoms,[1−3] 604 kJ mol^{-1} for UO_2^{2+}(g) and 746 kJ mol^{-1} for UO_2(g), is comparable to that for many transition-metal gaseous dioxides. However, ligands in the equatorial plane are weakly bound and labile.

There have been several authoritative reviews of the electronic structure of actinide compounds from a computational perspective.[4−7] A discussion with more experimental emphasis, focusing on actinyl ions, appeared in 1992;[8] this Feature Article is its sequel. At that time the optical spectroscopy of UO_2^{2+} and NpO_2^{2+} compounds was the main source of experimental data, but recently X-ray spectroscopy has thrown more light on the nature of the An−O bond. Moreover, the scope and power of theoretical methods has since been much enhanced. The inclusion of configuration interaction now enables dynamic electron correlation to be treated successfully, at least for the open-shell states accessible under optical excitation, whereas the ability to handle the spin−orbit interaction in addition to scalar relativistic effects has provided a comprehensive and largely satisfactory theoretical description of these states.

Finally, a number of new actinide compounds, containing actinyl-like triatomic structures, have been identified recently. This is the result of both innovative synthetic chemistry and the spectroscopic characterization of unstable molecules, both in the gas-phase and in inert-gas matrices. It therefore seems appropriate to present a contemporary description of this family of structurally related compounds.

The main chemical characteristics of actinyl ions and some relevant background material can be found in the previous article.[8] Figure 1 shows an energy level scheme for the molecular orbitals (MOs) that are most significant in the An−O bonding. In UO_2^{2+} the LUMOs are the $5f_\delta$ and $5f_\phi$ components of the 5f shell. They are excluded by their symmetry from participation in the U−O bond. Actinide ions possess two primary valence shells, 5f and 6d. Both can form σ and π bonds to oxygen. The four highest filled MOs, $3\sigma_g$, $3\sigma_u$, $1\pi_g$, and $2\pi_u$,

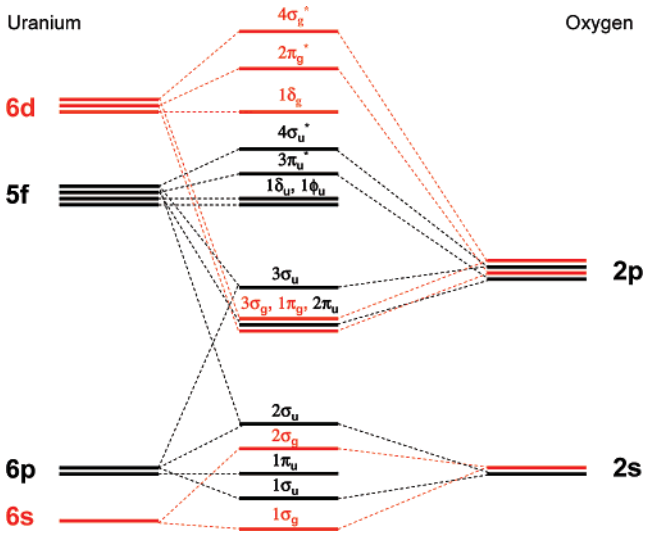

Figure 1. Schematic energies of actinyl valence orbitals.

nominally centered on the oxygen atoms, can be viewed as bonding and thus suggest a notional U−O bond order of three.

The relative importance of the σ_g, σ_u, π_g, and π_u components that comprise the bonding interactions is not obvious. The scheme in Figure 1 makes the familiar (but actually fallacious) assumption that σ-overlap exceeds π-overlap, but it is also unclear whether the different extent of the U(5f) and U(6d) overlaps with O(2p) will outweigh their energy difference in determining their contributions to the bond. The orbital basis must, however, also include the "pseudo-core" 6p electrons, because their XPES ionizations show large axial field splittings that correlate inversely with the U−O bond distance.[9] It is also usual to consider the 6*s* shell whose radial extension is comparable to that of 5f. Finally the O(2s) orbitals are included because of their near degeneracy to, and interaction with, U(6p). The MOs formed from this group of participating AOs are numbered accordingly in Figure 1. Note, however, the omission of actinide 7s and 7p, a policy that will, in due course, be seen to be not always tenable.

The many factors involved in the bonding can be largely unraveled by indentifying the apparent energies of all the participating valence orbitals, be they filled or empty. The

† E-mail: Bob.Denning@chem.ox.ac.uk.

10.1021/jp071061n CCC: $37.00
Published on Web 04/27/2007

Robert G. Denning was born in London, England, in 1938. He received his first degree in Chemistry from the University of Oxford in 1962 and a D.Phil., also from Oxford, in 1964, having worked under the direction of L.M. Venanzi. He became a Post-Doctoral research associate with the late T.S. Piper at the University of Illinois, Champaign-Urbana in 1964 and joined the Faculty there in 1966. In 1968 he was appointed to a Faculty position in the Inorganic Chemistry Laboratory at Oxford and has worked there since that time. In 1996 he was appointed Professor of Chemistry. He served as a consultant to the United Kingdom Atomic Energy Authority from 1974 to 1982. His research activities have been largely focussed on the optical properties of solids, and are described in more than 120 publications. Although focussing primarily on the electronic structure of actinide and lanthanide species, he has also worked on non-linear optic materials, as well as pioneering the application of two-photon spectroscopy to the solution of electronic structural problems in inorganic chemistry. More recently he has worked on the development of novel optical methods for the fabrication of 3-dimensional photonic crystals.

necessary electronic excitations can be divided into those in the optical region, and those at higher, i.e., X-ray, photon energies.

II. Experimental Work

II.1. Optical Electronic Excitations. *II.1.1. Principal Features.* In single crystals, advantage can be taken of polarized optical spectroscopy at low temperatures. Experiments on crystals of $Cs_2UO_2Cl_4$ and $CsUO_2(NO_3)_3$ and the analogous neptunyl(VI) species at ~5 K give very detailed spectra that have been comprehensively discussed and reviewed.[8] The crystal structures of these compounds locate the uranyl ion in sites close to D_{4h} and D_{3h} symmetry, respectively. More recently, the two-photon absorption spectrum (TPA) of $CsUO_2(NO_3)_3$ has confirmed the identity of the ten or so electronic excited states that are typically observed in the UO_2^{2+} spectrum between 20 000 and 32 500 cm^{-1}.[10] Within this group, state symmetries have been established by a variety of polarization measurements, and in several cases magnetic moments have also been determined.[8]

Taken as a whole, this large body of work shows that all of these excited states can be attributed to just two, parity-conserving, orbital excitations, i.e., $3\sigma_u \rightarrow 5f_\delta$ and $3\sigma_u \rightarrow 5f_\phi$. The excited configurations (abbreviated as $\sigma_u\delta_u$ and $\sigma_u\phi_u$) have average energies that are only weakly dependent on the nature of the equatorial ligands. They do, however, give rise to numerous excited states due to three perturbations of similar magnitudes: the spin−orbit interaction, the electron-correlation, and the equatorial ligand field. The properties of these states can all be modeled satisfactorily by an empirical perturbation Hamiltonian.[10]

Because the $5f_\delta$ and $5f_\phi$ orbitals are nonbonding with respect to oxygen, rather limited information about the U−O bond is available from these spectra, other than the identity of the HOMO. Nevertheless several features, which we now discuss,

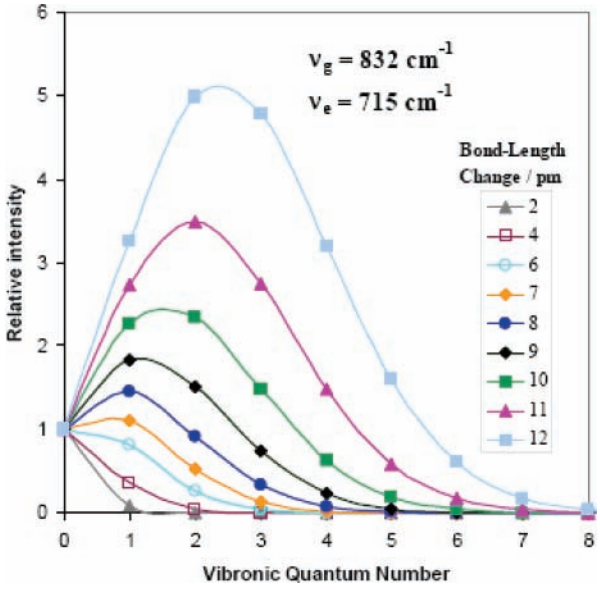

Figure 2. Relative intensities in excited state progressions.

can be used to test the validity of current theoretical techniques. (The term "HOMO" is used loosely to mean the orbital from which the lowest energy electronic excitation occurs. This need not correspond to the highest energy SCF MO.)

II.1.2. Excited State Bond Lengths. The high resolution of the spectra at low temperature[11] permits the determination of both excited state vibrational frequencies and bond lengths. Figure 2 shows computed relative intensities profiles for a progression in the O−U−O symmetric stretching mode.[12] These are a sensitive function of the change in the equilibrium U−O bond length. In the case of $Cs_2UO_2Cl_4$, spectra fitted to these profiles indicate that, relative to the ground state, all the excited states stemming from the $\sigma_u\delta_u$ and $\sigma_u\phi_u$ configurations experience a U−O bond elongation in the range (6.5−7.5) ± 0.5 pm. The most reliable values are those for the first two excited states, for which the elongation is 6.5 and 7.5 ± 0.2 pm, respectively.

In centrosymmetric chromophores TPA transitions conserve parity, so only electronic origin bands and their combination with even parity vibrational modes are observable. In most cases electron−phonon coupling does not induce TPA intensity, so the presence of these modes indicates changes in equilibrium geometry in the electronic excited state. The TPA spectrum of $Cs_2UO_2Cl_4$ is therefore much simpler than the linear absorption,[10,13] and the spectral contrast is so large (typically >1000) that even very weak vibronic features, such as the U−Cl symmetric stretching mode, can be identified. Two excited states (III and IV) in $Cs_2UO_2Cl_4$ exhibit this mode, with frequencies of 265 and 262 cm^{-1} at 5 K. In the ground state, at 300 K, the frequency is 264 cm^{-1}. Noting the temperature difference, it is safe to conclude that any decrease in frequency in the excited states is small. Relative to the origin bands these features are weaker by a factor of 0.03, from which it can be deduced that the U−Cl bond length of 267.1 pm[14] increases by 1.4 pm (0.53%) in the excited state. This is small compared to the ~7 pm (4%) increase in the 177.4 pm U−O bond length. Such weak features and small bond-length changes are not usually detectable in one-photon absorption, where vibronically induced electric-dipole intensity, from numerous *ungerade* modes, dominates and confuses the spectrum.

This result is striking because the redistribution of charge from the $3\sigma_u$ MO, notionally centered on oxygen, to the $5f_\delta$ and $5f_\phi$ orbitals, whose amplitudes are largest in the equatorial plane of the chloride ions, might be expected to substantially

increase the U−Cl bond length. For example, the small Huang−Rhys parameter[15] of 0.03 for the U−Cl stretch in these states can be contrasted with that for a 4d → 4d* excitation in *trans*-$[Rh(en)_2Cl_2]^+$ where the value for a 250 cm^{-1} Rh−Cl stretch is 21.[16] We will return to this result in section III.2.2.

In the TPA spectra of $CsUO_2(NO_3)_3$, in addition to the usual O−U−O progressions, there is evidence of a substantial modulation of the equatorial nitrate chelate angles in the excited states.[13] The $5f_\phi$ orbitals split in D_{3h} into a_1'' and a_2'' components; the former is σ-antibonding with respect to the nitrate oxygens and the latter π-antibonding. These are substantially stronger than the π-antibonding $5f_\delta$ interactions with the chloride ions in $Cs_2UO_2Cl_4$.

II.1.3. Configuration Interactions. The magnetic dipole intensity in origins near 20 096 and 26 222 cm^{-1} is informative because this transition mechanism is formally forbidden for all states in the $\sigma_u\delta_u$ and $\sigma_u\phi_u$ manifolds.[11] The estimated transition moments are 0.18 and 0.15 μ_B. They signal the presence of spin−orbit and tetragonal field interactions that link the $\sigma_u\delta_u$ and $\sigma_u\phi_u$ configurations, respectively, with the $\sigma_u3\pi_u$ configuration to which magnetic-dipole transitions are allowed. The magnetic-dipole transition moment for an atomic $f_\sigma \rightarrow f_\pi$ transition is 3.46 μ_B, so the small observed moments reflect, for example, (a) the $\sigma_u\pi_u$:$\sigma_u\delta_u$ configuration interaction coefficient that is of order $(\sqrt{10}/2)(\zeta/\Delta E) \approx 0.2$, where ζ is the spin−orbit coupling constant, and (b) a transition moment that is reduced from the 5f one-center value by the composition of the $3\sigma_u$ MO.

Further configuration interactions are apparent in a pair of states in $Cs_2UO_2Cl_4$ found at 27 720 and 27 758 cm^{-1}. The second-order Zeeman effect unambiguously establishes the symmetry of these states as Γ_g in $D_{\infty h}$ and A_{2g} and A_{1g}, respectively, in D_{4h}.[11] Substantial magnetic-dipole intensity polarized *parallel* to O−U−O is found in the A_{1g} component. Analysis shows that both the 38 cm^{-1} splitting and the magnetic-dipole intensity can be explained only if these states, which are primarily derived from the $\sigma_u\phi_u$ configuration, contain some $2\pi_u^3\phi_u$ character.[17] The $\sigma_u\phi_u$:$\pi_u^3\phi_u$ interaction is a consequence of spin−orbit coupling between the $3\sigma_u$ and $2\pi_u$ orbitals, and the magnetic dipole intensity is due to the tetragonal field perturbation that links the A_{1g} component of the $\pi_u^3\phi_u$ configuration with the ground state.

II.I.4. Other Orbital Energies. Two additional valence orbitals can be located by optical spectroscopy. The f−f transitions of the $5f^1$ NpO_2^{2+} ion can be unambiguously identified. They establish that the f_π−f_ϕ separation is 1.59 eV in $Cs_2NpO_2Cl_4$ and 1.74 eV in $CsNpO_2(NO_3)_3$.[8] It is unlikely that these energies differ much from those in the uranyl analogs. The increased effective nuclear charge of Np could strengthen the covalent bonds and increase the f_π−f_ϕ separation. However, in practice the reduction of the O−An−O symmetric stretching frequency from 832 cm^{-1} in $Cs_2UO_2Cl_4$ to 802 cm^{-1} in $Cs_2NpO_2Cl_4$ suggests that this is offset by a more contracted, core-like 5f-shell. The core contraction is apparent in the bond distances of the isomorphous compounds $Cs_2UO_2Cl_4$ and $Cs_2NpO_2Cl_4$. The An−O distances of 177.4(4) and 175.8(22), and the An−Cl distances of 267.1(1) and 265.7(5) pm, respectively, indicate a contraction of ∼1.5 pm.[14,18,19]

In $Cs_2NpO_2Cl_4$ the 37 cm^{-1} reduction in the NpO_2 stretching frequency from 802 cm^{-1} in the "f_δ/f_ϕ" ground state to 765 cm^{-1} in the $5f_\pi^*$ excited states is modest compared with the 120 cm^{-1} reduction when a $3\sigma_u$ valence electron is excited into the 5f shell. Apparently, the f_π^* orbitals are rather weakly antibonding.[20] The relative progression intensities in this mode indicate that the Np−O bond length increases in the excited state by 4.9 pm.

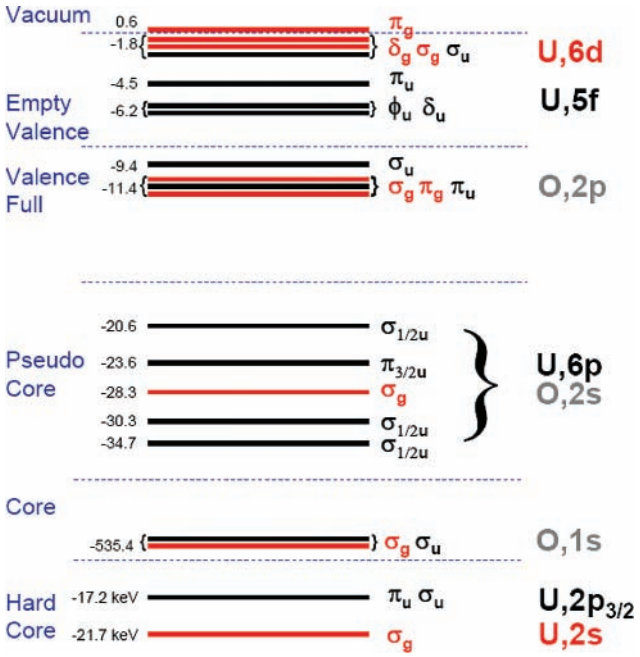

Figure 3. Experimental orbital energies in $Cs_2UO_2Cl_4$: *gerade* states, red; *ungerade* states, black.

Finally, the polarized excited state absorption spectrum of $Cs_2UO_2Cl_4$ can be used to locate the filled $3\sigma_g$ valence orbital ∼2.0 eV below $3\sigma_u$.[21] The $3\sigma_g \rightarrow 3\sigma_u$ transition leads to a further decrease in the U−O frequency to 585 cm^{-1}, and the absorption band profile indicates a large increase in the U−O bond length to 195 pm.[21,22]

II.I.5. Optical Spectroscopy—Summary. Figure 3 shows the energies of several orbitals obtained from the optical data. It also includes some core and pseudo-core orbitals, whose energies will be considered shortly. Note, however, that in multi-electron systems orbital energies are not observables, rather they have the imprecise status of SCF eigenvalues. Although Figure 3 is approximate, because it assumes that orbital energies can be directly deduced from ionization or excitation energies, we will, nevertheless, use these energies to illustrate the main features of the chemical bonding.

Employing Koopmans' approximation, one can deduce the absolute energy of the $3\sigma_u$ HOMO in $Cs_2UO_2Cl_4$ from photoelectron spectroscopy to be −9.4 eV, although there is some uncertainty, perhaps as much as ±0.5 eV, in this value.[8] The transition energies determined above are averaged and rounded, where necessary, to obtain the orbital energies in Figure 3. In this way the $3\sigma_g$ valence orbital is located at −11.4 eV, the f_δ orbital at −6.3 eV, the f_ϕ orbital at −6.05 eV and, assuming that f_π−f_ϕ separation is equal to that in $Cs_2NpO_2Cl_4$, the f_π orbital at −4.46 eV.

Hitherto the determination of the energies of other valence orbitals has been frustrated by two factors. First, the photoelectron spectrum of the filled valence shell is overlaid by ionizations from the equatorial ligands,[23] and second, the optical spectrum in the ultraviolet is rendered intractable by charge-transfer excitations to uranium from these same ligands. However, these obstacles can be partially overcome by means of X-ray spectroscopy. Core excitations have an unambiguous energy and, below the ionization threshold, terminate at vacant MOs that have a substantial presence on the atom containing the core hole.

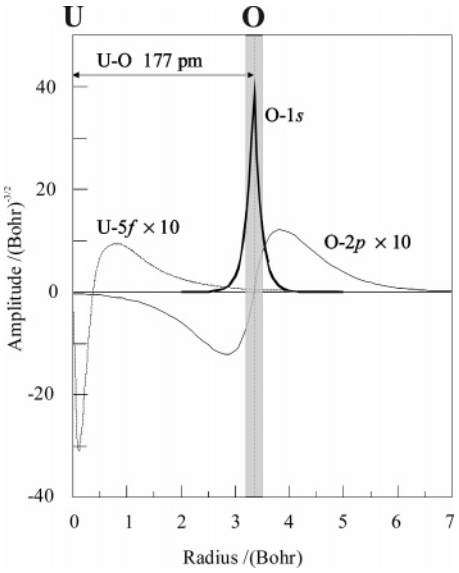

Figure 4. Radial amplitude functions in UO_2^{2+}. Reprinted with permission from Denning, R. G.; Green, J. C.; Hutchings, T. E.; Dallera, C.; Tagliaferri, A.; Giarda, K.; Brookes, N. B.; Braicovich, L. *J. Chem. Phys.* **2002**, *117*, 8008−8020.[24] Copyright 2002, American Institute of Physics.

Figure 3 includes the energies and symmetries of some core and "hard core" orbitals suitable for the current purpose.

II.2. X-ray Spectroscopy. The oxygen (Kα/1*s*) absorption and emission, near 530 eV, is particularly informative, in part because the lifetime of the 1s hole contributes only ∼0.2 eV to the spectral width. In $Cs_2UO_2Cl_4$ the only oxygen atoms are those within the uranyl ion, and the crystal structure, containing one molecule per primitive unit cell, makes it straightforward to obtain polarized X-ray absorption spectra (XAS).[24] The interpretation of the oxygen 1s XAS is illustrated in Figure 4, which shows radial wavefunction amplitudes for the O(1*s*), O(2p), and U(5f) orbitals.

If *z* is the displacement from the oxygen nucleus in the U−O direction, the intensity of excitations from O(1*s*) to O(2p) or U(5f) orbitals is determined by transition moments with the form $\langle\psi_{2p}|e\mathbf{z}|\psi_{1s}\rangle$ and $\langle\psi_{5f}|e\mathbf{z}|\psi_{1s}\rangle$. The product $e\mathbf{z}|\psi_{1s}\rangle$ has extrema of opposed sign separated by ∼16 pm, so the relative magnitude of the transition moments depends on the *gradients* of the O(2p) and U(5f) functions primarily within this small region (shaded in Figure 4) close to the oxygen nucleus. The O(2p) contribution to the intensity is estimated to be ∼3000 times larger than that from U(5f).[24]

The absorption intensity is then effectively proportional to the square of the O(2p) coefficient in the empty uranium-centered MOs and is a useful measure of covalency. The O(1s) XAS spectra of transition-metal oxides illustrate how the density of vacant "3d" states can be mapped by this technique;[25] the ligand field splittings agree closely with those obtained by optical spectroscopy.

II.2.1. Oxygen Kα Absorption Spectroscopy. The polarized spectrum of $Cs_2UO_2Cl_4$ is shown in Figure 5. For technical reasons the polarizations are incomplete,[24] but clearly there are three sharp transitions, centered at 531.4, 534.1, and 536.5 eV. The first and last are polarized perpendicular to O−U−O, and the strong central feature is polarized parallel to this axis. The photoelectron spectrum of $Cs_2UO_2Cl_4$ places the O(1s) orbital energy 526.0 eV below the HOMO.[23] However, in section II.1.4 the $5f_\pi^*$ level was found to lie 5.0 eV above $3\sigma_u$ (Figure 3). The O(1s) → $5f_\pi^*$ transition should therefore give rise to a perpendicular polarized absorption near (526 + 5) = 531 eV, and clearly corresponds to the band at 531.4 eV. Transitions to the vacant $5f_\delta$ and $5f_\phi$ orbitals near 529.5 eV are forbidden, except for a small (∼2%) mixing with $5f_\pi^*$ induced by the spin−orbit interaction and the tetragonal ligand field: they are too weak to observe.

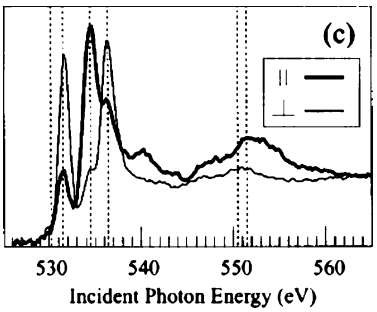

Figure 5. Polarized O Kα absorption spectrum of $Cs_2UO_2Cl_4$. Reprinted with permission from Denning, R. G.; Green, J. C.; Hutchings, T. E.; Dallera, C.; Tagliaferri, A.; Giarda, K.; Brookes, N. B.; Braicovich, L. *J. Chem. Phys.* **2002**, *117*, 8008−8020.[24] Copyright 2002, American Institute of Physics.

TABLE 1: Calculated and Experimental O Kα Excitation Energies and Intensities

final state molecular orbital	$5f_\pi$(u)*	$5f_\sigma$(u)*	$6d_\sigma^*$(g)	$6d_\pi^*$(g)
$UO_2Cl_4^{2-}$ excited state energies/eV (calc).	531.44	534.13	534.30	535.81
$UO_2Cl_4^{2-}$ excited state energies/eV (expt)	531.4	534.1	∼534	536.5
rel intensity (calc)	0.36	1.00	0.17	0.79
rel intensity (expt)t	∼0.6	1.0	?	∼1.1

A scalar relativistic (ZORA) DFT calculation, employing the BP86 functional, helps to clarify the assignment of the remaining features.[24] Transition energies were obtained from the difference between the total SCF energy of the ground state of $UO_2Cl_4^{2-}$ and that of a configuration having a hole in O(1s) and an electron in the relevant MO. The results are shown in Table 1. On this basis, the perpendicularly polarized O(1s) → $6d_\pi^*(2\pi_g)$ transition is naturally assigned to the band at 536.5 eV.

Transitions to $6d_\sigma^*(4\sigma_g)$ and $5f_\sigma^*(4\sigma_u)$ should be parallel-polarized; that to $6d_\sigma^*$ is predicted to be very weak (Table 1) compared with that to $5f_\sigma^*$ with which it is nearly degenerate. We therefore presume that they are not spectrally separable and that $5f_\sigma^*$ is the dominant source of parallel intensity near 534 eV. This conjecture is supported by good agreement between the experimental and calculated energies for the three main bands in Table 1. We then obtain the following (virtual) orbital energies: $6d_\sigma^* = 5f_\sigma^* = -1.8$ eV, $6d_\pi^* = +0.6$ eV. These are included in Figure 3 with the same reservations as before.

II.2.2. O Kα Emission Spectroscopy (XES).[24] Additional information is available from the polarized emission spectrum in Figure 6. Two sample orientations were used. In the first, the O−U−O direction is nearly parallel to the optic axis of the emission spectrometer, and only emission polarized perpendicular to O−U−O can be detected. In the second case the O−U−O axis is nearly perpendicular to the emission spectrometer axis, so **both** parallel and perpendicularly polarized transitions can be observed.

The spectra were obtained under excitation at 531.4 eV. Weak elastic (Rayleigh) scattering at this energy is clearly visible. If the core hole refills radiatively from $3\sigma_u$, the initial and final states differ only by a one-electron excitation from $3\sigma_u$ to $3\pi_u^*(5f_\pi^*)$—an electronic Raman process whose energy is close to 5.0 eV (see above). Emission from $3\sigma_u$ should therefore occur

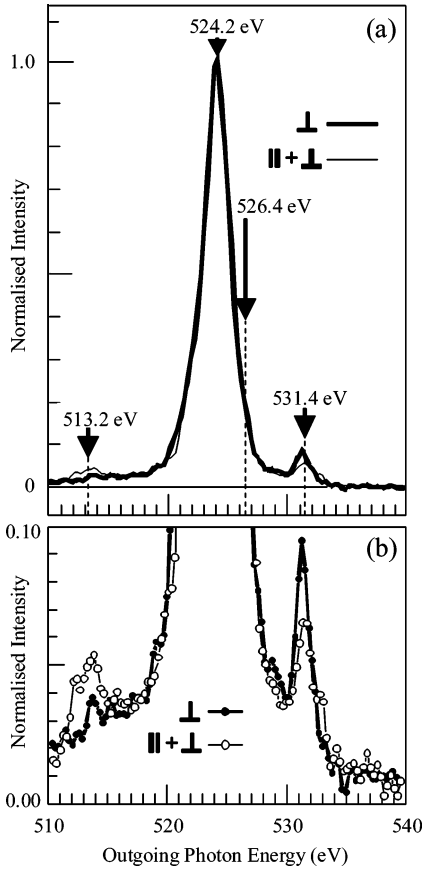

Figure 6. O Ka emission spectra of $Cs_2UO_2Cl_4$. Reprinted with permission from Denning, R. G.; Green, J. C.; Hutchings, T. E.; Dallera, C.; Tagliaferri, A.; Giarda, K.; Brookes, N. B.; Braicovich, L. *J. Chem. Phys.* **2002**, *117*, 8008−8020.[24] Copyright 2002, American Institute of Physics.

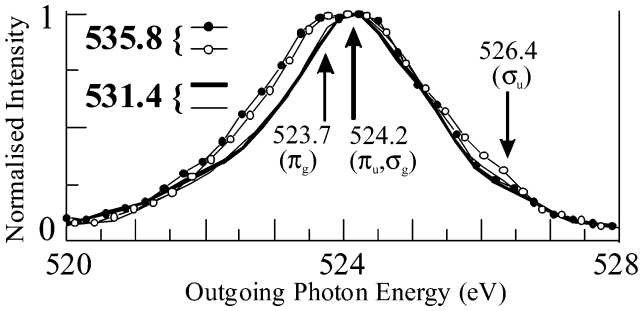

Figure 7. O Kα emission spectra at two excitation energies. Polarizations as in Figure 6. Reprinted with permission from Denning, R. G.; Green, J. C.; Hutchings, T. E.; Dallera, C.; Tagliaferri, A.; Giarda, K.; Brookes, N. B.; Braicovich, L. *J. Chem. Phys.* **2002**, *117*, 8008−8020.[24] Copyright 2002, American Institute of Physics.

close to 526.4 eV. The absence of significant intensity at this energy in Figure 6, shows that the oxygen 2p character of $3\sigma_u$ is small compared to that of the other valence orbitals at lower energy.

The XES also shows small excitation dependent shifts (Figure 7).[24] Excitation at 531.4 eV populates the $5f^*_\pi$ orbitals and creates a *gerade* core hole, so emission should only occur from $3\sigma_u$ and $2\pi_u$. The strong feature at 524.2 eV is therefore assigned to $2\pi_u$. In contrast, excitation at 535.8 eV to the $6d^*_\pi$ level creates an *ungerade* hole. The emission spectrum is now noticeably broader and may indicate the presence of two components. From the optical data on the $3\sigma_g \rightarrow 3\sigma_u$ transition, the higher of these (at 524.2 eV) is near the energy expected for $3\sigma_g$ emission, so the spectrum suggests that $1\pi_g$ emission is

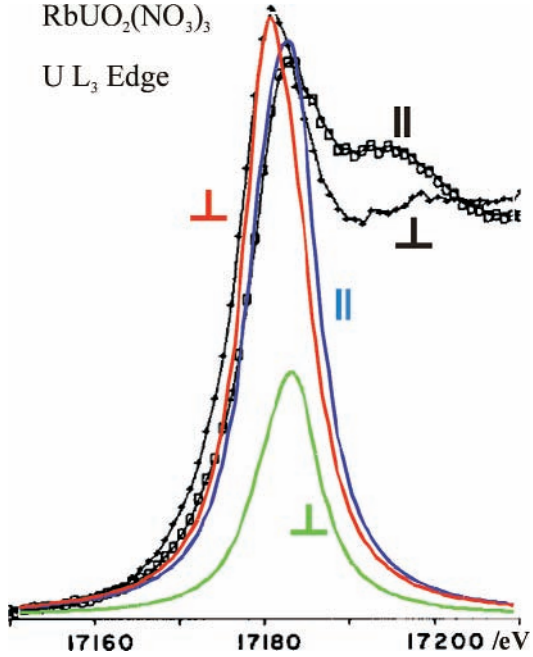

Figure 8. Experimental (black) and simulated (color) polarized XAS, after Templeton and Templeton.[27] Reprinted with permission from Templeton, D. H.; Templeton, L. K. *Acta Crystallogr.* **1982**, *A38*, 62−67.[27] Copyright 1982, International Union of Crystallography.

centered ∼0.5 eV to lower energy. Given the width of these features and the absence of any detectable polarizations in Figure 7 these assignments must be taken as tentative. For this reason the $3\sigma_g$, $1\pi_g$, and $2\pi_u$ orbitals have been assigned the same nominal energy (−11.4 eV) in Figure 3.

Finally, we consider the weak feature at 513.2 eV in Figure 6. This occurs with the correct (parallel) polarization and in the correct energy region to correspond to emission from the $\sigma_{1/2u}$ spinor component of the $6p_{3/2}$ atomic level in the "pseudo-core", which must therefore possess some O(2p) character. This is direct evidence for covalent bonding by this shell and complements that from the analysis of XPES axial field splittings.[9] The 6p levels in the Figure 3 carry spinor labels because the spin−orbit interaction in this penetrating shell is very large (∼5 eV).[26] Their energies and that of 6*s* were obtained by matching the XPES data[23] with the energies predicted by a four-component Dirac-Hartree−Fock calculation.[26]

II.2.3. Uranium L_3 Edge XAS. The $6d_\delta$ valence orbitals, as yet unlocated, are nonbonding with respect to oxygen. They interact with, and are split by, the tetragonal field of the chloride ions in $UO_2Cl_4^{2-}$, but angular momentum conservation makes them inaccessible from O(1s). We therefore turn to the "hard-core" U(L_3, $2p_{3/2}$) shell from which transitions, near 17.2 keV (cf. Figure 3), are allowed to *all* the 6d orbitals. The polarized spectrum of a single crystal of $RbUO_2(NO_3)_3$, measured by the Templetons,[27] is shown in Figure 8. Despite the "natural" line width of 7.43 eV,[28] there is marked linear dichroism. The first peak is perpendicularly polarized with a maximum 2.1 eV below the main parallel-polarized absorption.[27] Transitions from $2p_{3/2}$ to vacant s and d shells are electric-dipole allowed, but the intensity of the former should be isotropic, so the dichroism in this region reflects the splitting of the 6d shell. Figure 8 overlays the experimental spectra with a simulation (red and blue) that assumes the 7.43 eV line width and also that $6d_\sigma$ and $6d_\delta$ are degenerate and lie 3.5 eV below $6d_\pi$. Instrumental broadening is ignored, and the relative intensities are calculated using atomic uranium wavefunctions.[24] In $Cs_2UO_2Cl_4$, $6d_\sigma$ and $6d_\delta$ are calculated to be nearly degenerate and to occur ∼2.0 eV below $6d_\pi$.[24]

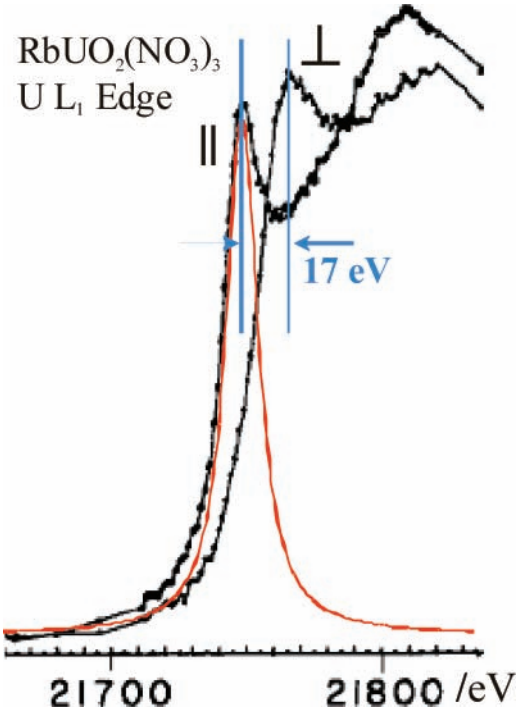

Figure 9. Experimental and simulated XAS. Reprinted with permission from Templeton, D. H.; Templeton, L. K. *Acta Crystallogr.* **1982**, *A38*, 62−67.[27] Copyright 1982, International Union of Crystallography.

The equatorial field is of course different in $RbUO_2(NO_3)_3$ so only approximate agreement should be expected. Nevertheless, the simulated and experimental spectra agree very satisfactorily, the peak separation of 2.1 eV being the same as that observed experimentally. Figure 8 also includes a simulated perpendicularly polarized spectrum (green) from which transitions to the $6d_\delta$ orbitals have been excluded. It is clear from the effect of omitting these orbitals that they are the *main* source of perpendicular intensity in the lowest energy transition. These results confirm the near degeneracy $6d_\delta$ and $6d_\sigma$ as well as their relationship to $6d_\pi$ and these energies are incorporated in Figure 3.

II.2.4. Uranium L_1 Edge XAS. Finally, we consider the U-2s (L_1) XAS. Only orbitals with uranium np character are accessible from this shell. The highly dichroic spectrum of $RbUO_2(NO_3)_3$ is shown in Figure 9 together with a simulation employing a line width of 14 eV.[28] The polarized spectrum of a uranyl acetate dihydrate crystal is very similar[29] so this dichroism is intrinsic to the uranyl ion. Although the reported instrumental width is ~2 eV,[27] the data are fitted better by a total width of 14 + 4 = 18 eV (not shown). The first band at 21 745 eV is strongly parallel polarized, but the 17 eV anisotropy between the main peaks is far too large to attribute to the axial field splitting of a vacant 7p shell. If the splitting of this shell were small compared to the line width, the spectrum would not be strongly polarized. This paradox can be resolved by observing that, although the σ_u and π_u components of 5f and 6p orbitals share the same symmetry in $D_{\infty h}$, only the σ_u components are strongly mixed in the empty $5f_\sigma^*(4\sigma_u^*)$ molecular orbital at −1.8 eV (Figure 3). This orbital then has the substantial $6p_\sigma$ character needed to explain the strong parallel polarized L_1 edge intensity. In contrast, the $6p_\pi$ coefficient in the $5f_\pi^*$ MOs, which determines the perpendicularly polarized intensity, is negligible.

II.3. Experimental Data Summary. Figure 3 summarizes the available orbital energy data. Note that **all** the filled and empty valence orbitals of significance have been located spectroscopically, although there is some uncertainty in the relative energies of the filled $3\sigma_g$, $1\pi_g$, and $2\pi_u$ orbitals. We reiterate that this diagram is not exact. Virtual orbital energies cannot be deduced directly from transition energies, due to changes in electron-correlation energy. In practice, however, relativistic DFT calculations suggest that, at least for the virtual orbitals accessed by X-ray spectroscopy, the error introduced by assuming that an excitation energy is equal to an orbital energy difference can be quite small (i.e., <0.5 eV).[24]

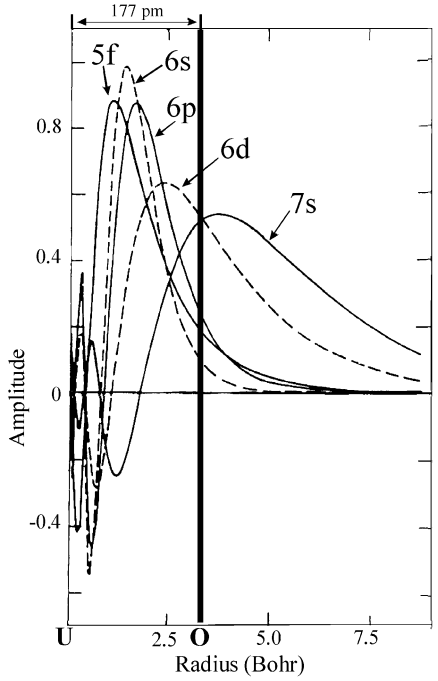

Figure 10. Radial amplitudes in the uranium atom.

With these reservations, the spectroscopic data and the energy levels in Figure 3 suggest the following main features of the electronic structure:

(1) Whereas the $5f_\pi^*$ molecular orbitals are weakly antibonding, the "$5f_\sigma^*$" antibonding interaction is much more significant, raising the energy of this orbital by a further 2.7 eV. The L_I XAS spectra imply that "$5f_\sigma^*$" is a strongly mixed hybrid of $5f_\sigma$ and $6p_\sigma$.

(2) The $6d_\pi^*$ MO's are substantially more antibonding than the $6d_\sigma^*$.

(3) The $3\sigma_u$ HOMO, although bonding, is much less so than $3\sigma_g$, $1\pi_g$, and $2\pi_u$. It also has less oxygen 2p character.

(4) There is direct spectroscopic evidence for covalent participation by U(6p) in the σ_u components of the valence orbitals.

III. Theoretical Studies

III.1. Valence Orbital Properties. *III.1.1. Radial Wavefunctions.* The radial amplitudes of the actinide orbitals influence their role in the actinyl bond. Figure 10 shows the results of an atomic relativistic calculation.[30] Notice that the 5f "valence" orbitals are more contracted than the "pseudo-core" 6p, but that 6d and 7s are much more diffuse, extending well beyond the position of the oxygen nucleus.

III.1.2. Overlap Integrals. Values of the U−O overlap integrals for the $UO_2Cl_4^{2-}$ ion, calculated using an all-electron scalar relativistic (ZORA) DFT method,[24] are collected in Table 2. They are related to the radial amplitude distributions in Figure 10. In the 5f shell π-overlap is much larger than the σ-overlap—a difference that is even more pronounced in the 6d shell. This

TABLE 2: Overlap Integrals in $Cs_2UO_2Cl_4$.

	6p		5f		6d		7s
	σ_u	π_u	σ_u	π_u	σ_g	π_g	σ_g
O(2p)	0.257	0.115	0.070	0.142	0.075	0.312	0.061
O(2s)	0.238		0.152		0.414		0.276

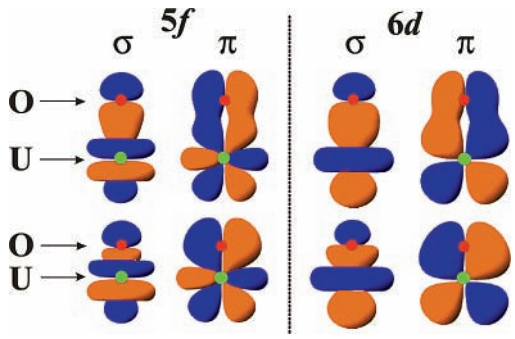

Figure 11. MO amplitudes, showing oxygen 2p overlap at two U−O distances (uses *Orbital Viewer* David Manthey 2004).

unfamiliar result was first established many years ago.[31,32] Its origin is shown schematically in Figure 11, which illustrates the MO densities at two U−O distances.

For both $5f_\sigma$ and $6d_\sigma$ a cancellation of positive (orange) amplitude in the overlap region becomes very pronounced at short distances, but this does not occur for $5f_\pi$ and $6d_\pi$. This happens because the $O(2p_\sigma)$ overlap with the positive (orange) axial lobe of $5f_\sigma$ is largely cancelled by that from the negative (blue) toroidal lobe, which therefore appears thinner than its positive counterpart. It is also clear in Figure 10 that $6d_\sigma$ and $7s_\sigma$ are so diffuse that they overlap both positive and negative regions of $O(2p_\sigma)$. The resulting cancellation for $6d_\sigma$ at short distances can be seen in Figure 11. Neither of these factors applies to the more contracted 6p shell where, as is more usual, $S(6p_\sigma) > S(6p_\pi)$. The cancellation of $O(2p_\sigma)$ overlap due to the diffuseness of $6d_\sigma$ and $7s_\sigma$ is, as expected, absent in their overlap with O(2s). The O(2s) orbitals, although less important, should not be ignored because they are close in energy to $U(6p_\sigma)$ and overlap well with it (cf. Table 2).

III.2. DFT Calculations. *III.2.1. Geometry and Bond Lengths.* DFT calculations on actinide compounds offer a stringent test of the Kohn−Sham orbitals and functionals required to handle relativistic effects and exchange−correlation energy in heavy atom systems.[5,7,33] Because these methods variationally optimize the electron density represented by a single determinant SCF wavefunction, they cannot be expected to describe excited states satisfactorily. Applications therefore focus on ground state geometries, bond lengths, and vibrational frequencies in species such as $[UO_2X_4]^{2-}$, where X = F, Cl, and OH[5,34] or in the hypothetical compounds where X = CN[35] or CO,[36] as well as on isomerization pathways.[37,38] A comparison of the performance of DFT methods, for a number of actinyl species and their analogs, with that of computationally expensive multireference Hartree−Fock (HF) methods such as CASPT2, support their validity.[39]

Many applications seek to predict the properties of complexes in aqueous solution such as the set with composition $[UO_2(H_2O)_m(OH)_n]^{2-n}$ ($n + m = 5$) that exist at different pH values,[40−42] as well as the mechanism of water exchange in the penta-aquo complex which, for an ion of this size, is quite slow ($\sim 10^6$ s^{-1}).[43−45] Solvation effects can now be handled with sufficient accuracy to predict aqueous reduction potentials for the $[AnO_2(H_2O)_5]^{2+}/[AnO_2(H_2O)_5]^{+}$ (An = U, Np and Pu) couple to within 0.5 V of the experimental value.[41] To achieve this, it is essential to incorporate the spin−orbit interaction, whose magnitude in the 5f shell is of the order of 0.25 eV, as an *ad hoc* correction. Effective core potentials (section II.3.1) which treat 78 electrons (i.e., up to an including 5d) as part of a "large core", give much poorer results than "small-core" potentials that simulate the field of 60 electrons.[41]

III.2.2. Valence Orbital Energies. Several authors report DFT valence MO energies. These should be indicative of the various orbital contributions to the U−O bond. Typical values for the isolated UO_2^{2+} ion *relative* to the $3\sigma_u$ HOMO, are $3\sigma_g$ −0.71 eV, $2\pi_u$ −1.28 eV, and $1\pi_g$ −1.57 eV.[46] Slight variations are obtained from different DFT methods,[36,47] but all predict the same orbital ordering and overall energy span. The large separation between the $3\sigma_u$ HOMO and the other orbitals is attributable to the contribution from the pseudo-core 6p shell, which raises the energy of $3\sigma_u$ as a result of "pushing from below", a notion that has been widely discussed elsewhere.[4,6,8,46,48] The relatively small bonding contribution from $3\sigma_u$ is apparent in quite small changes in the U−O bond length (+7.5 pm) and the O−U−O symmetric stretching frequency (−120 cm^{-1}) when an electron is excited from it (section II.1.2), compared with an excitation from $3\sigma_g$ where the equivalent values are +17.6 pm and −245 cm^{-1} (section II.1.4).

In the presence of a set of equatorial ligands, $3\sigma_u$ remains well above the other orbitals in this group, but their order changes. In Kaltsoyannis's study of $[UO_2(H_2O)_m(OH)_n]^{2-n}$ ($n + m = 4$, 5) the *relative* energy of $3\sigma_g$ is shifted down to an extent proportional to the number of hydroxy groups, whereas the relative energies of $2\pi_u$ and $1\pi_g$ are almost unchanged.[40] In $[UO_2(OH)_4]^{2-}$ the energy of $3\sigma_g$ is lowered by ~1.25 eV, making it easily the most stable of this group of orbitals. Both $3\sigma_g$ and $2\pi_u$ orbitals have no nodes in the equatorial plane and can therefore form σ-bonds to the equatorial ligands.[40] At the 233 pm distance of the equatorial ligands, the σ-overlap of $6d_\sigma$ exceeds that of the more contracted $5f_\pi$, so the main influence of these ligands is on the energy of $3\sigma_g$. The hydroxide ion being a better donor than water, has a frontier orbital energy above those of the uranyl fragment, thereby stabilizing $3\sigma_g$ by an amount proportional to the number of H_2O ligands that are replaced by OH^- groups.

The equatorial ligand interaction typically increases the energy span of the valence orbitals from ~1.5 eV in the isolated ion to ~2.1 eV, in good agreement with estimates derived from XPES and from the O Kα emission spectrum. For $UO_2Cl_4^{2-}$ a similar re-ordering is found, although in this case $3\sigma_g$ is only 0.06 eV below $1\pi_g$.[24] For this species the chlorine $3p_\sigma$ overlap integrals with $6d_\sigma$ and $5f_\pi$ are 0.18 and 0.05, respectively, so the primary influence of the equatorial chloride ligands is again to depress the energy of $3\sigma_g$.

III.2.3. Virtual Orbital Energies. The overlap integrals in Table 2 are consistent with the observation (Figure 3) that the more antibonding $6d_\pi$ ($2\pi_g^*$) orbital occurs ~2.4 eV above $6d_\sigma$ ($4\sigma_g^*$). On the other hand, they seem to conflict with the fact that $5f_\sigma(4\sigma_u^*)$ is found ~2.7 eV **above** $5f_\pi(3\pi_u^*)$.

An explanation can be found in the form of the $4\sigma_u^*$ wavefunction, in which the main AO coefficients are $U(5f_\sigma)$ +0.756, $U(6p_\sigma)$ +0.712, and $O1(2p_z) = O2(2p_z)$ +0.642. Note that $5f_\sigma$ and $6p_\sigma$ have nearly equal weight and are in-phase. When superposed (hybridized), their amplitudes add on-axis but cancel at polar angles between the conical nodes of $5f_z3$ at $\theta = 39.2°$ and 140.8°. A schematic representation of this superposition is shown on the left side of Figure 12. The large $U(6p_\sigma)$ contribution (implied by the U L_1 data in section II.2.4), with $S_{O(2p)} = 0.258$ (Table 2), greatly increases the effective overlap

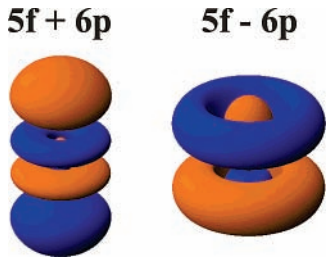

Figure 12. $5f_\sigma$ and $6p_\sigma$ hybrid orbitals (uses *Orbital Viewer* David Manthey 2004).

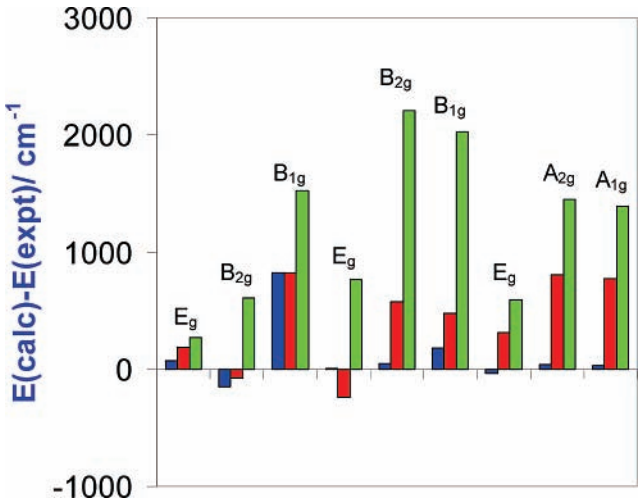

Figure 13. Energy deviations in $Cs_2UO_2Cl_4$ using empirical[13] (blue), MRCI-SOC[49] (green), and CASPT2-SOC[53] (red) methods.

relative to that of $5f_z3$, for which $S_{O(2p)} = 0.070$. The phases of O1 and O2($2p_z$) are antibonding with respect to this $5f_\sigma/6p_\sigma$ hybrid, and the interaction is sufficiently strong to place the 4 σ_u^* orbital 2.7 eV above $3\pi_u^*$, due primarily to the contribution from $6p_z$. On the other hand, in the $3\pi_u^*$ orbital, the main coefficients are U($5f_{\pi x}$) +0.9024 and O1($2p_x$) = O2($2p_x$) −0.389 and, due to its small overlap, the $6p_{\pi x}$ contribution is negligible. The O(2p) coefficients confirm the much reduced covalency in $3\pi_u^*$ compared to $4\sigma_u^*$. These calculations are therefore in good agreement with the conclusions drawn from the XAS energies and intensities in section II.2.1.

III.3. Multireference Methods. *III.3.1. Methodology.* The open-shell optical excited states of the uranyl ion provide numerous observables that are more revealing than the ground state properties. Theoretical treatments therefore need to make use of multireference configuration interaction (MRCI) methods, i.e., those that take as their starting point wavefunctions variationally optimized in a multi-configurational (MCSCF) SCF calculation. This is an important prerequisite for CI calculations if they are to successfully account for electron correlation in excited states. To date there have been two technically distinct treatments of these states in actinyl compounds.

Pitzer's group has investigated the properties of UO_2^{2+} and NpO_2^{2+} both as isolated species and in the environment provided by the $Cs_2UO_2Cl_4$ crystal.[49−52] They use the relativistic effective core potential (RECP) approximation, whereby the wavefunctions of the chemically inert core electrons, obtained from a Dirac−Fock relativistic atomic calculation, serve to define a core potential. The valence orbitals are replaced by pseudo-orbitals that are radially nodeless within the core and have characteristics defined by this potential. The MOs were first optimized by carrying out a MCSCF calculation, in which the

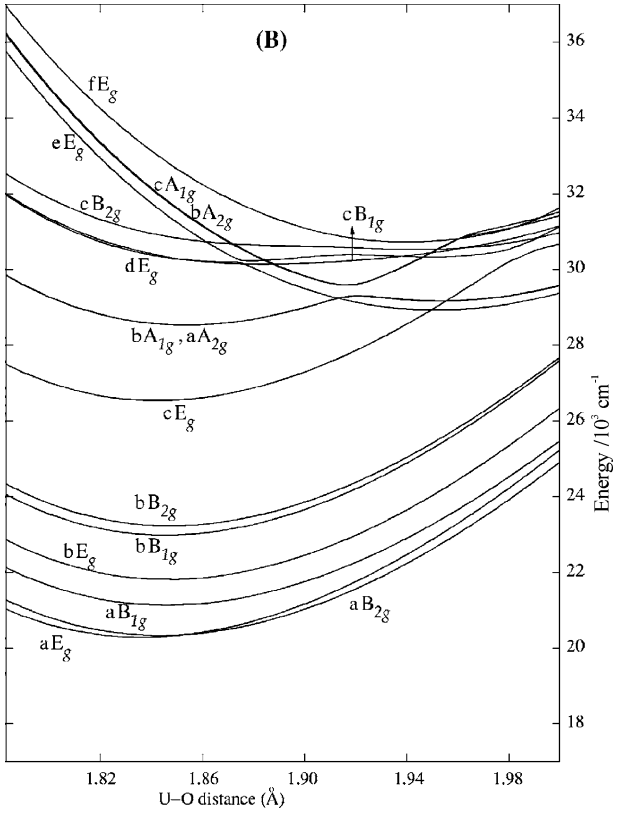

Figure 14. Potential energy curves for the excited states of $Cs_2UO_2Cl_4$. Reprinted with permission from Pierloot, K.; van Besien, E. *J. Chem. Phys.* **2005**, *123*, 204309.[53] Copyright 2005, American Institute of Physics.

energies of the ground state and six excited states were averaged. The valence electrons were then treated by a multireference CISD method that incorporates both the electron−electron repulsion and the spin−orbit interaction. For example, the nearly degenerate $\sigma_u\delta_u$ and $\sigma_u\phi_u$ configurations, both of which have $\omega = (5/2)$ components (in the $\omega-\omega$ limit), are strongly mixed by spin−orbit coupling (SOC) and are conveniently treated in this way. The spin−orbit interaction and the electron−electron repulsion, which are of comparable magnitude in these excited states, are handled simultaneously—a potentially more accurate procedure than treating them sequentially. On the other hand, this MR-SOC-CI method requires such a large number of CI states that it is necessary to freeze a subset of the electrons in the active space.

An alternative all-electron approach, due to Pierloot and van Besien,[53] treats the *scalar* relativistic interactions of the core electrons using the Douglas−Kroll Hamiltonian,[53] and employs a basis set specifically adapted to this Hamiltonian.[54] Multireference MOs are derived by the complete active space CASSCF method, which permits the inclusion of all possible configurations generated by excitations within a selected set of real and virtual valence orbitals (that define the active space). Configuration interactions arising from the electron−electron repulsion are then handled perturbatively (up to second order) by the CASPT2 method,[55] and the resulting "spin−orbit free" (SOF) eigenvalues are used as diagonal energies in the spin−orbit Hamiltonian matrix. The SOC is therefore treated *a posteriori*, using the restricted active space state interaction (RASSSI) method, the Hamiltonian being constructed and diagonalized within the CASSCF basis.[56] This stepwise procedure means that it is not possible to fully account for any orbital relaxation associated with the spin−orbit interaction. However, in the 5f

TABLE 3: Experimental and Calculated Energies, Vibrational Frequencies, and Bond Lengths

	T_e/cm^{-1}			ω_e/ cm^{-1}			R_e(U−O)/pm		
	expt	CASPT2	SOC-CI	expt	CASPT2	SOC-CI	expt.	CASPT2	SOC-CI
X A_{1g}	0	0	0	832	819	968	177.4	178.3	172.8
a E_g	20 096	20280[a]	20363	715	712	885	183.9	183.6	179.0
b B_{2g}	20407	20330	21013	710	703	879	184.9	184.4	179.2
a B_{1g}	21316	21139	21838	696	698	878	184.9	184.6[a]	179.0
b E_g	22051	21809	22819	711	711	874	184.9	184.6	179.4
b B_{1g}	22406	22984	24618	717	721	902	184.9	184.6	180.6
b B_{2g}	22750	23228	24780	711	714	900	184.9	184.7	180.6
c E_g	26222	26534	26817	725	722	904	184.9	184.2	180.5
a A_{2g}	27720	28527	29169	705	703	896	184.9	185.4	180.8
b A_{1g}	27757	28530	29145	708	703	890	184.9	185.4	180.7

[a] Corrected values.

shell, the SOC is small compared to that in more penetrating valence shells with lower values of *l*, so this approach has been tested successfully in several heavy-atom molecules..[56] Nevertheless, insofar as the 6p shell is an important contributor to the actinyl valency, the neglect of the much larger (∼5 eV) spin−orbit interactions within this shell could be a source of significant error.

III.3.2. Excited State Properties. The results of these MR-SOC-CI and CASSCF/CSAPT2 calculations are compared in Figure 13, which shows the differences between the calculated and experimental energies for the first nine electronic excited states of $Cs_2UO_2Cl_4$. Pitzer et al.[49] include a detailed evaluation of the full crystal field potential that is quite successful in accounting for the (small) splittings that arise from the actual C_{2h} uranium site symmetry, whereas Pierloot and van Besien[53] use the idealized D_{4h} symmetry of an isolated $UO_2Cl_4^{2-}$ ion. The averages of the C_{2h} component energies[49] are used for the comparison in Figure 13.

The results from an empirical Hamiltonian that includes the $\sigma\pi_{3/2}$ configuration in the spin−orbit Hamiltonian,[13] are also included in this figure. Both SCF calculations somewhat overemphasize the excited state energies, T_e, but the ordering of the states and their general agreement with experiment is impressive. However, the CASSCF/CASPT2 calculation is notably more accurate, a difference that has been attributed to the use of an overlarge effective core potential in the MR-SOC-CI calculations.[53]

Both theoretical treatments also calculate the O−U−O vibrational frequencies, ω_e, and equilibrium bond lengths, R_e(U−O), in $Cs_2UO_2Cl_4$. These are compared to experimental values in Table 3 (corrections supplied by the original author). The CASPT2 calculation reproduces the experimental values of ω_e with impressive accuracy. The experimental bond distances R_e(U−O) are in most cases indistinguishable from 184.9 ± 0.3 pm, although the distance in the first (a E_g) excited state is clearly shorter by ∼1 pm (section II.1.2). These values are also well reproduced, but the method is somewhat less successful in the ground state, underestimating the O−U−O frequency by 13 cm^{-1} and overestimating the bond length by 0.9 pm. It is also clear from this table that the SOC-CI (RECP) calculation[49] gives ω_e values that are substantially too high and bond distances that are too short—features that can also be attributed to the shortcomings of the effective core potential.[57]

Figure 14 shows potential energies as a function of the symmetric O−U−O coordinate for the $UO_2Cl_4^{2-}$ anion, calculated by the CASPT2 method.[53] A group of excited states, with much larger equilibrium bond lengths is found above 29 000 cm^{-1}. These possess a large degree of $\pi_u^3\delta_u$ and $\pi_u^3\phi_u$ character. Extensive vibronic mixing between configurations takes place in this region, giving complex energy surfaces that are consistent with the large spectroscopic bandwidths found in this part of the spectrum.[13] The $\sigma_u\phi_u$:$\pi_u^3\phi_u$ interactions match the experimental observations in section II.1.3. In states dominated by the $\pi_u^3\delta_u$ and $\pi_u^3\phi_u$ configurations, the equilibrium U−O distances are close to 196.0 pm. The increase of 18.6 pm relative to the ground state is large compared to that found in the $\sigma_u\delta_u$ and $\sigma_u\phi_u$ states. As in the case of $3\sigma_g$ (section III.2.2), the $2\pi_u$ orbitals are clearly more strongly bonding than $3\sigma_u$, as expected from their orbital energies (Figure 3).

Although the performance of the CASSCF/CASPT2 calculation is impressive, it omits a significant part of the CI. The SOC Hamiltonian matrix includes the ground state and SOF states derived from the $\sigma_u\delta_u$, $\sigma_u\phi_u$, $\pi_u^3\delta_u$ and $\pi_u^3\phi_u$ configurations, but not those from the $\sigma_u\pi_u^*$ configuration.[53] Yet it is clear from the magnetic-dipole intensity (section II.1.3) that interaction with this configuration is significant. Using DFT MO coefficients[24] and 5f-shell eigenvectors obtained by diagonalizing an empirical Hamiltonian that includes the $\sigma_u\pi_u^*$ configuration, one calculates the transition near 20 096 cm^{-1} to have a magnetic moment of 0.24 μ_B, a figure that compares well with the observed value of 0.18 μ_B. On this basis the inclusion of the $\sigma_u\pi_u^*$ configuration should selectively lower the energy of those states with predominantly $\sigma_u\delta_{u(3/2)}$ character (in the $\omega-\omega$ limit) by ∼300−400 cm^{-1}. Furthermore, the additional π-antibonding character should increase their equilibrium bond distances and lower their O−U−O frequencies. Clearly, future theoretical work ought to include interactions with this configuration.

Zhang and Pitzer make an important observation about the effect of CI.[51] The largest contributors to the excited states are indeed the $3\sigma_u\delta_u$ and $3\sigma_u\phi_u$ configurations, the population of $3\sigma_u$ being ∼50% uranium centered, but there are also major contributions from the $2\sigma_u\delta_u$ and $2\sigma_u\phi_u$ configurations, where $2\sigma_u$ is predominantly the pseudo-core $6p_\sigma$ orbital. When the admixture of these configurations is taken into account, the hole in the highest energy $3\sigma_u'$ (the prime indicating the mixed or "rotated" composition) orbital becomes even more metal centered at the expense of O(2p), thereby reducing the extent of oxygen to uranium charge transfer involved in the excitation. At the same time the CI results in an increase in the O(2p) content of $2\sigma_u$. This partly compensates for the charge transfer accompanying the excitation from $3\sigma_u$, so that a population analysis finds essentially the *same* charge on oxygen in the excited states as it does in the ground state. This observation agrees well with the absence of any significant change in the distance of the equatorial ligands in the excited states, and the invariance of their stretching frequency (section II.1.2). The reduced O(2p) character in the $3\sigma_u$ orbital arising from the configuration interaction is also in satisfactory agreement with the small O Kα emission intensity at the energy expected for emission from this orbital (section II.2.2 and Figure 6).

TABLE 4: Energies and Mulliken Populations (%) of Occupied Valence Orbitals in $Cs_2UO_2Cl_4$

orbital	energy/eV	6p	5f	6d	O($2p_\sigma$)	O($2p_\pi$)	Cl($3p_\sigma$)	Cl($3p_{\pi v}$)	Cl($3p_{\pi h}$)
a_{2u}	0.81	**4**	**16**		**18**			**63**	
a_{2g}	0.79								100
e_g	0.69					10		89	
b_{1u}	0.45		5					94	
e_u	0.35		6				3		89
e_u	0.20	2	3			4	85		5
b_{2g}	−.17			11					89
a_{2u} ($3\sigma_u$)	−0.32	**5**	**32**		**25**			**35**	
a_{1g}	−0.54			1	21		72		
b_{1g}	−0.64			12			84		
e_u ($2\pi_u$)	−1.04		**27**			**70**	**3**		
e_g ($1\pi_g$)	−1.62			**18**		**72**		**9**	
a_{1g} ($3\sigma_g$)	−1.68			**13**	**64**		**17**		

III.3.3. Higher Energy Configurations. Pierloot has calculated the SOF energies of the various states of $UO_2Cl_4^{2-}$ that arise from the $\sigma_u\delta_u$, $\sigma_u\phi_u$, $\pi_u^3\delta_u$, $\pi_u^3\phi_u$, $\sigma_g\delta_u$, $\sigma_g\phi_u$, $\pi_g^3\delta_u$, and $\pi_g^3\phi_u$ configurations. Considering only configurations of the type $\gamma\delta_u$, the average of configuration energies *relative to* $\sigma_u\delta_u$ are $\pi_u^3\delta_u$ 1.71 eV, $\pi_g^3\delta_u$ 1.95 eV, and $\sigma_g\delta_u$ 2.07 eV. Pierloot notes the apparent inversion of the ordering of $3\sigma_g$ and $1\pi_g$ orbital energies relative to the case of the isolated UO_2^{2+} ion, for which the $\sigma_g\delta_u$ configuration is calculated to lie 0.65 eV *below* $\pi_g^3\delta_u$. Though this inversion can be understood in terms of the role of the Cl($3p_\sigma$) interaction with $3\sigma_g$, as discussed in section III.2.2, it raises two problems. First, Pierloot indicates that the chloride population in the valence orbitals is minimal. Second, it becomes difficult to understand the excited state absorption spectrum, which is consistent with a parity-allowed $\sigma_u\delta_u \rightarrow \sigma_g\delta_u$ transition centered near 2.2 eV. The energy of this transition is well reproduced by Pierloot's calculation. However, the $\sigma_u\delta_u \rightarrow \pi_g^3\delta_u$ transitions are predicted to occur at only a slightly ($\sim$1000 cm^{-1}) lower energy, in a region where no appropriately polarized intensity is found experimentally. It is difficult to see why this transition should be weak, so this inconsistency remains unresolved.

III.4. Equatorial Ligand Interactions and Excitations. Theoretical studies vary in their description of the composition of the filled valence orbitals in the ground state of the $UO_2Cl_4^{2-}$ ion. Matsika and Pitzer use a Mulliken population analysis to find an overall negative charge of 0.75 on the chloride ions in $Cs_2UO_2Cl_4$ and note that **none** of the uranyl valence orbitals ($3\sigma_u$, $3\sigma_g$ $2\pi_u$, and $1\pi_g$) "mix significantly" with chlorine orbitals.[49] Similarly, Pierloot's CASPT2 calculations on $UO_2Cl_4^{2-}$ find very small chlorine contributions to these orbitals; specifically, the Mulliken populations are $3\sigma_u$ 1%, $3\sigma_g$ 2%, $2\pi_u$ <1%, and $1\pi_g$ 6%.[53] This calculation is made on the isolated $UO_2Cl_4^{2-}$ ion and may therefore underestimate the positive potential at the chloride ions in relation to the actual crystal potential in $Cs_2UO_2Cl_4$ (which is treated comprehensively in Pitzer's work[49]).

The results of a recent DFT calculation, which uses the BP86 (LSDA/GGA) exchange−correlation functional, on the $UO_2Cl_4^{2-}$ ion[24] are shown in Table 4. Those orbitals whose symmetry and composition indicate that they have a major role in the U−O bond are presented in boldface type. Chlorine $3p\pi$ orbitals are directed in either the vertical (v) or horizontal (h) directions with respect to the C_4 axis.

According to this calculation the seven highest energy orbitals are primarily centered on the chloride ions, and the lowest three on oxygen. Most orbitals with significant metal content involve *either* O(2p), as in the case of the lowest energy $e_u(2\pi_u)$ and $e_g(1\pi_g)$, or Cl(3p) (b_{2g} and b_{1g}) in which case only the 6d interactions are important. Exceptions, however, are found for the pairs of a_{1g} and a_{2u} orbitals. In the former case there is substantial mixing between Cl($3p_\sigma$) and O($2p_\sigma$). Their in-phase combination, at −0.54 eV, has a small net overlap and interaction with $6d_\sigma$, but the out-of-phase combination ($3\sigma_g$) has enhanced overlap with $6d_\sigma$, thereby lowering the MO energy to −1.68 eV. This interaction is responsible for the stability of this orbital in $[UO_2(OH)_4]^{2-}$ (section II.2.2).[40]

The two a_{2u} orbitals are comprehensive mixtures of U($5f_\sigma$), U($6p_\sigma$), O($2p_\sigma$), and Cl($3p_{\pi v}$) although the lower of the two has more oxygen and less chlorine character and is therefore labeled $3\sigma_u$. They differ in that the π-interaction between the chloride ions and the out-of-phase hybrid of $6p_z$ and $5f_z3$ is antibonding in the HOMO at 0.81 eV but bonding in $3\sigma_u$. This hybrid, represented schematically on the right-hand side of Figure 12, has little amplitude on the *z*-axis, but enhanced amplitude in its interaction with Cl($3p_{\pi v}$). The lowest energy optical excitations, which leave a partial hole in this hybrid, would thus tend to shorten the U−Cl distance. The excited electron, however, enters the $5f_\delta$ and $5f_\phi$ orbitals whose interaction with the equatorial ligands is weakly π-antibonding. The balance of these two factors appears to be responsible, together with the small change in oxygen population, for the negligible change in U−Cl bond length.

Although the populations in Table 4 contrast with the much more ionic character found by Pierloot[53] and Pitzer,[49] this discrepancy is not unexpected. In the case of the $CuCl_4^{2-}$ anion, DFT local and nonlocal exchange−correlation functionals, such as BP86, have been compared with hybrids (e.g., B3LYP) that include a degree of HF exchange.[58] The experimental spin-density data show that when pure DF exchange is employed, the covalency of the Cu−Cl bond is substantially overemphasized, and the bond is predicted to be too long by 10 pm. On the other hand, a hybrid functional that includes 38% HF exchange reproduces the experimental ionic character satisfactorily, shortens the Cu−Cl bond by 3 pm, and predicts charge-transfer transition energies in good agreement with experiment. It appears that the inherent self-interaction of the approximate exchange−correlation functionals overstabilizes the metal orbitals in relation to those of the chloride.[58] In $Cs_2UO_2Cl_4$ the BP86 functional overestimates the U−O bond length by 4 pm and the U−Cl bond length by 7 pm.[24] It would therefore be valuable to study actinyl−equatorial ligand interactions with a hybrid functional comparable to that used for $CuCl_4^{2-}$.

Because the HOMOs in Table 4 are chlorine-centered, it might seem that the lowest energy excitations should be charge-transfer transitions from chloride to uranium, but this is obviously at variance with the optical spectroscopy.[8] Within a SCF-LCAO model, if no orbital relaxation is permitted, the energy of an excitation from orbital *a* to orbital *b* is given by

$$W_{ab} = \epsilon_b - \epsilon_a - (J_{ab} - K_{ab}) \pm K_{ab} \qquad (1)$$

where ϵ_a and ϵ_b are their SCF energies, J_{ab} and K_{ab} have their usual meaning, and the positive (negative) sign is associated with the singlet (triplet) state.[59] For states arising from the $\sigma_u\delta_u$ or $\sigma_u\phi_u$ configurations K_{ab} is too small ($\sim$0.3 eV)[10] to concern us. The main correction to the orbital energy difference is the Coulomb interaction between the electron localized in the $5f_\delta$ and $5f_\phi$ orbitals and the hole in the orbital from which it was excited. For a full electron transfer from an ionic chloride orbital to the δ_u or ϕ_u orbital localized on uranium (over 267.1 pm) the electron−hole interaction energy is $\sim$3.3 eV, whereas for a hole localized on oxygen at 177.4 pm it would be $\sim$5 eV. However, if the excitation takes place from a valence orbital with substantial uranium 5f character J_{ab} is much larger. For example a multiconfiguration Dirac−Fock calculation on the U^{4+} ion gives a 5f−5f Coulomb energy of $\sim$18 eV.[60] The 5f−6d Coulomb integrals, relevant to excitations from *gerade* bonding orbitals, are very much smaller,[60] as would expected from the diffuseness of 6d. These energies will not be quantitatively correct, as they ignore orbital relaxation. Nevertheless, configurations generated by excitations from valence orbitals with substantial 5f orbital character are expected to be stabilized relative to those that correspond to Cl → U charge transfer.

Thus, although the HOMO's seem to be largely chlorine centered, the first charge-transfer states of $Cs_2UO_2Cl_4$ have been calculated by Matsika and Pitzer to lie at energies greater than 33 000 cm^{-1}—a full 1.6 eV above the first excited states.[49] This is compatible with the onset of an intense broad absorption at 23 000 cm^{-1} in $Cs_2UO_2Br_4$ crystals,[61] and typical differences of $\sim$1 eV in the threshold energies of chloride-to-metal and bromide-to-metal charge transfer.[62] Superficially, the DFT MOs in Table 4 appear unsatisfactory in ascribing substantial chloride character to the $3\sigma_u$ orbitals in the ground state, because an excitation from orbitals with this composition could lead to a substantial change in U−Cl bond length in the excited state. However, because the excited electron is localized in a $5f_{\delta,\phi}$ orbital, Equation 1 implies that the most stable excited configuration will maximize J_{ab} and, if other factors are equal, should place a hole in an orbital whose composition has enhanced 5f character relative to that in the ground state. Excited state CI should therefore give added weight to configurations in which a σ_u hole occupies an orbital with much reduced chlorine character relative to that in the ground state. If this is the case, the U−Cl bond could be almost unaffected by the excitation. It would be useful to investigate the subtlety of this point by explicit examination of the excited state wavefunctions, and by computing potential energy surfaces for the U−Cl stretching coordinate.

III.5. Nuclear Electric Field Gradients. The evidence for the participation of the 6p shell in the U−O bond gave rise to the suggestion[63] that the resulting anisotropy of the electron density in this shell, associated with a partial hole of $\sim$0.33e^- in the $6p_z$ orbital,[49] might be responsible for the electric field gradient (EFG) at the actinide nucleus. This property has been measured by Mössbauer spectroscopy[64,65] in compounds containing $^{237}NpO_2^{2+}$ and $^{234,236,238}UO_2^{2+}$. For $RbUO_2(NO_3)_3$ the axial component of the EFG is $+8.14 \times 10^{18}$ V cm^{-2}.[64]

However, all actinide shells with $l > 0$ that participate in the An−O bond, not just 6p, should exhibit some anisotropy in their charge distribution as a result of the covalency. Relativistic CCSD(T) calculations[26] on the isolated UO_2^{2+} ion, show that the EFG is the result of incomplete cancellation between a large *positive* contribution from a partial $6p_z$ (axial) core hole, and large *negative* contributions from the additional (axial) electron density in the $6d_\sigma$, $6d_\pi$, $5f_\sigma$, and $5f_\pi$ orbitals. The latter arise because U−O covalency preferentially adds axial electron density to the 5f and 6d shells. The EFG calculated in this way is positive but rather too small.[26] Better agreement with experiment is obtained in calculations that allow the donation from the equatorial ligands in $RbUO_2(NO_3)_3$ to add electron density to the $6d_\delta$ and $5f_\phi$ orbitals in the equatorial plane.[66] The reduced anisotropy in the population of these shells accentuates the *positive* contribution from the 6p core hole.

The results of this work[66] typically come within a factor of 2 of the experimental value. However, the fact that there is only one experimental observable but many different contributions to the EFG, each of which is a sensitive to different components of the bonding, makes this an inconclusive test of theoretical methodology.

III.6. Inverse Trans Influence (ITI). This concept was introduced in 1992.[8] It is based on a comparison of bond lengths in six-coordinate species of the type MZY_5^{n-}, where Z is either an oxo or nitrido group and Y is a halide. If M is a $d^{0,1,2}$ metal, the $M-Y_{trans}$ bond is typically **longer** than $M-Y_{cis}$ by 5−15%. In transition-metal chemistry, if Z is a strongly bound ligand, this type of elongation is called a trans Influence. On the other hand, in the two available actinide examples with Z = O, Y = Cl, and M = U or Pa, the $M-Y_{trans}$ distances are 4−8% **shorter** than the $M-Y_{cis}$ distances. Unfortunately, there is no other suitable diffraction data, so the remainder of the evidence for the ITI is more indirect.

In $CsUOF_5$ disorder in the complex anion orientation prevents the determination of bond lengths by diffraction methods. However, in the solid state ^{19}F NMR spectrum the trans fluorine is found 120 ppm downfield of the four cis fluorines, indicating that the bond to it is more covalent.[69] An analysis of the vibrational spectrum is also consistent with a substantially larger stretching force constant in the $U-F_{trans}$ bond.[70]

In another example, the low-temperature optical absorption and emission spectra of $(PPh_4)UOCl_5$ show well-resolved progressions in both the U−O and $U-Cl_{trans}$ stretching modes.[71] In the electronic ground state the $U-Cl_{cis}$ symmetric stretching frequency occurs at 293 cm^{-1}, but the $U-Cl_{trans}$ mode is found at 345 cm^{-1}. The Huang−Rhys factors indicate that, in the excited state, the hole is in an orbital having substantial interactions with both the oxo group and the trans chloride ligand, and that the cis chlorides are unaffected. Bagnall found that whereas the four cis chlorides are instantaneously replaced by bromide in HBr/CH_2Cl_2 solutions, the replacement of the trans chloride takes several hours.[72] These observations suggest the presence of linear partially covalent OUF^{3+} and $OUCl^{3+}$ groups that share some of the robustness of actinyl ions.

The original rationalization of the ITI was qualitative,[8,71] but the Kaltsoyannis group has now made a quasi-relativistic DFT study of a series of compounds with the composition $AnOY_5^-$ (An = Pa, U, Np; Y = F, Cl, Br).[73] They predict a preferential shortening of the $U-Y_{trans}$ bonds by about 2%, rather less than is found in the (sparse) experimental data.[8] Similar results have recently been reported by Chermette et al. .[74] In both sets of calculations the bond distances are only satisfactory if the local density approximation is used.[73,74] Chermette's work predicts a **normal** trans influence not only in molybdenum analogs but also in $UOCl_5^-$ *provided* that the 5f shell is artificially removed from the bonding by raising its energy by 25 eV.[74] Apparently then ligand interactions with the 5f shell are a central feature of the ITI. This point is supported by Kaltsoyannis' finding that the ITI increases in the sequence $UOBr_5^- < UOCl_5^- < UOF_5^-$

< $NpOF_5$, consistent with a lowering in energy of the 5f orbitals, as the positive charge on the actinide increases, thus enhancing their participation in the U−O bond. Kaltsoyannis also finds that the larger part of the ITI, but not all of it, is absent if the pseudo-core 6p orbitals are "frozen" in the SCF procedure and thus excluded from participation in the bond.

A simplified orbital analysis of the factors underlying the ITI focuses on the role of two axially symmetric MOs ($6a_1$ and $9a_1$). Both are bonding toward oxygen but have σ^* interactions with the trans halide and π^* interactions with the cis halides.[73] The higher energy $9a_1$ orbital involves substantial out-of-phase hybridization of $5f_\sigma$ and $6p_\sigma$, already discussed in section III.4 (cf. Figure 12). The effect of the addition of 6p character is thus to enhance π^* interactions with the equatorial ligands, and decrease σ^* interactions with the trans halide. Because the metal-orbital content of this orbital *increases* in the order $UOBr_5^-$ < $UOCl_5^-$ < UOF_5^- < $NpOF_5$, its composition appears to be an important factor in the computed increase in the ITI in this series.

The $6a_1$ orbital, in contrast, contains little $6p_\sigma$ character, more $5f_\sigma$, and a larger amount of $6d_\sigma$. The resultant f−d hybrid is mainly directed toward the U−O bond and has some cancellation of amplitude in the direction of the *trans* halide, so that antibonding interactions in this direction are small. The metal content of this orbital *decreases* in the order $UOBr_5^-$ > $UOCl_5^-$ > UOF_5^-, and the cis ligand p_π content increases. Given the antibonding nature of the metal halide interactions, it is clear that this orbital also plays a part in the ITI.

Analogous computational results have been reported for UX_4 (X = F, Cl, Br, I) molecules,[75] although no experimental structural data are available for comparison. It appears that the lowest energy geometry has C_{3v} symmetry. Typically, the axial U−X bonds are computed to be 2−4% shorter than the equatorial bonds and the ITI is again most pronounced in the fluoride.

IV. Structural Analogs

IV.1 Diimido Compounds. The imido group, R−N$^-$, and the oxide ion are formally isoelectronic. In the d-block transition metals, the chemical similarity between oxo (M = O), imido (M = N−R), and phosphorane-iminato (M = N−PR_3) compounds is well established,[76,77] as are methods for their preparation and interconversion.[77−79] Although imido complexes of U(IV) have been known for some time,[80] until recently complexes of uranium(VI) have been rare, apparently requiring stabilization by bulky organometallic coligands.[81−83] More specifically, the *trans*-diimido structural unit, the formal analog of the uranyl ion, was unknown.

The main obstacles to the preparation of imido compounds are the ease of hydrolysis to the very stable dioxo species, and the possibility that the lower electronegativity of the imido group could result in spontaneous reduction to U(IV). However, in the past few years, viable synthetic routes to these species have been discovered.

IV.1.1. Synthesis and Properties. Phosphorane-iminato complexes can be made from the mono-oxo precursor $[UOCl_5]^-$ by reaction with a trimethylsilyl compound such as $Me_3SiNPAr_3$ or $Me_3SiNSAr_2$, where Ar is an aromatic group, to give $[UOCl_4(NPAr_3)]^-$, $[UOCl_4(NSAr_2)]^-$, or $UCl_4(NPAr_3)_2$.[84−86] These compounds contain trans O═U═N− and −N═U═N− groups that are structural analogs of the uranyl ion. However, the generality of this preparation is limited: if the phosphine substituents are too strongly electron donating, the uranium is reduced.[85]

Remarkably though, Boncella's group has discovered that simple *trans*-bis(alkyl or arylimido) compounds can be made by oxidizing $UI_3(THF)_4$ with iodine in the presence of Et_3N and a primary amine such as aniline.[87,88] The triethylamine deprotonates aniline, presumably assisted by its coordination to uranium, to give $U(NPh)_2I_2(THF)_3$. With *tert*-butylamine the product is $U(N\text{-}t\text{-}Bu)_2I_2(THF)_2$. The recent characterization of the $UO_2I_4^{2-}$ ion[89] supports the notion that a mild oxidant such as iodine can generate these formally U(VI) compounds, provided that the positive charge on uranium is moderated by strongly covalent oxo or nitrido ligands.

The equatorial ligands can be readily exchanged, although two iodides are always present. Interesting examples are $U(N\text{-}t\text{-}Bu)_2I_2(pyr)_2$ and $U(N\text{-}t\text{-}Bu)_2I_2(Ph_3PO)_2$, which adopt an all-trans (pseudo-D_{2h}) geometry, as well as the phosphine complex $U(N\text{-}t\text{-}Bu)_2I_2(PMe_3)_2(THF)$. Typical U−N bond lengths are close to 184 pm, somewhat longer than the uranyl U−O distance, which is usually close to 177 pm, but much shorter than the 191 pm U−N distance in the phosphorane-iminato species.[84]

$U(N\text{-}t\text{-}Bu)_2I_2(PMe_3)_2(THF)$ is the first phosphine complex of uranium(VI) to have been characterized—there are no uranyl analogs. Boncella notes the implied increase in the "softness" of the uranium(VI) coordination chemistry in the diimido species compared with the typical "hard" ionic interactions of the dioxo cation.[87,88] This softness is also supported by the observation that all the diimido species isolated so far contain coordinated iodide ions.

The bond distances in $U(N\text{-}t\text{-}Bu)_2I_2(Ph_3PO)_2$ can be usefully compared with those in $UO_2I_2(Ph_3PO)_2$ for which there are recent structural data.[90] The replacement of oxo by imido groups leads to a significant increase of 3.9(3) pm in the distances to *both* the iodide and phosphine oxide "spectator" ligands. This suggests a decreased positive charge on uranium due to a greater covalency in the U−imide bond compared to the U−O bond. The increased uranium character of the filled valence orbitals is also consistent with the stability of complexes containing π-acceptor ligands—it will be interesting to see whether this is sufficient to stabilize CO complexes.

Boncella has also recently reported the preparation and structure of a mixed oxo−imido analog, i.e., $U(N\text{-}t\text{-}Bu)OI_2(Ph_3PO)_2$.[91] Here the U−oxo and −imido distances are 176 and 182 pm, respectively, in good agreement with their values in the dioxo and diimido compounds. In this case the average U−phosphine oxide and U−I distances are larger by 2.1 and 0.7 pm than in the dioxo compound, suggesting an effective size for the uranium atom intermediate between that in the dioxo and diimido species.

IV.1.2. Electronic Structure. The $R_3P{-}N{=}U{=}N{-}PR_3$[46] and −N═U═N− class of compounds[87,88] have both been studied by DFT methods. Boncella's work includes a geometry optimization for $U(NMe)_2I_2(THF)_2$. The agreement between the calculated bond lengths and angles and experimental values in the *tert*-butyl analog is excellent. Both DFT studies arrive at the same important conclusion: the ordering of the four key valence orbital energies changes from $3\sigma_u > 3\sigma_g > 2\pi_u > 1\pi_g$ in the isolated UO_2^{2+} ion to $2\pi_u > 1\pi_g > 3\sigma_u > 3\sigma_g$ when the oxygens are replaced by imido or iminato groups.

The main effect of the replacement is to raise the energies of the π orbitals (of both parities) relative to those of the σ orbitals. If small splittings due to the C_{2v} symmetry are ignored, in $U(N\text{-}t\text{-}Bu)OI_2(Ph_3PO)_2$, the orbital energy order is $\pi(N) > \sigma(O) > \pi(O) > \sigma(N)$, the 2p orbitals of the atom in parentheses being the dominant contributor to the MO. The HOMO is again a

π-type orbital centered on the imido nitrogen atom, but the oxygen-centered MOs retain the usual order, i.e., $\sigma > \pi$.

The origin of this orbital reordering is clarified by Kaltsoyannis' DFT analysis,[46] which compares UO_2^{2+} with the isoelectronic UN_2. As expected for the less electronegative nitrogen ligand, the energies of all valence orbitals rise relative to the nonbonding uranium $5f_\phi$, but their order is maintained. However, in the imido species an axial σ-bond, using the nitrogen $2p_\sigma$ orbital, is made by the formal addition of H^+, R^+ (or in the case of the $R_3P-N{=}U$ compounds, R_3P^{2+}), so that the $2p_\sigma$ are preferentially stabilized, leaving a $2p_\pi$ HOMO. Alternatively, one can view the evolution of the isoelectronic U=O group into the U=N−H group as the notional relocation of an oxygen nuclear proton to the site of the H atom. Even if no electronic polarization were to accompany the redistributed nuclear potential, it should be obvious that, in response to the reduced nuclear charge, the $2p_\pi$ orbital energies will rise more than the $2p_\sigma$. This difference is accentuated if $2p_\sigma$ electrons occupy an MO with H−(1s) character and can "follow" the proton toward its new position.

Several other features emerge from this theoretical work. (i) As in the uranyl ion, the *cis*-diimido configuration is much less stable than the *trans*-diimido,[87,88] (ii) the imido compounds are notably more covalent than the dioxo species, as judged by the metal population in the filled valence orbitals,[87,88] and (iii) for the $R_3P-N{=}U$ compounds the total energy is almost independent of the U−N−P angle.[46] An equivalent absence of stiffness in the R−N−U angle in the diimido compounds is also suggested by the bending of the *t*-Bu group away from bulky ligands in the equatorial plane to give U−N−C angles of ~168°.[87]

IV.1.3. Optical Spectroscopy. The optical spectra of these compounds bear little resemblance to those of uranyl analogues. The diimido compounds are variously described as orange, red-orange, brown, or red-brown, compared to the pale yellow of uranyl compounds,[87,88] and "the vibronic coupling fine structure often seen in uranyl UV−vis spectra is not observed". Similarly, the R_3P-N-U compounds are described as red or red-orange.[85]

Brown reported the onset of a steadily rising *featureless* absorption for a solution of $U(NPTol_3)_2Cl_4$ near 750 nm and an extinction coefficient that reaches 1200 M^{-1} cm^{-1} at 500 nm.[92] The red-shifted absorption is consistent with the reduced HOMO−LUMO gap indicated by the DFT calculations.[46] At 15 K the $[PPh_4]^+$ salt of $[UO(NP(C_6D_5)_3)Cl_4]^-$ when excited at 532 nm shows a very weak, broad, *featureless* emission band centered at 720 nm.[86,93] In contrast, uranyl compounds in solution show numerous resolved bands forming progressions in the O−U−O stretching frequency between 500 and 350 nm with extinction coefficients that are typically <20 M^{-1} cm^{-1}. Luminescence, displaying sharp vibronic structure, also occurs efficiently at room temperature.

IV.1.4. Excited State Geometry. Boncella has suggested that the absence of clear vibronic progressions in the U=N stretching mode is due to its coupling to internal ligand modes of similar frequency. An alternative hypothesis is that, in the first electronic excited state at equilibrium, the U−N−R group is bent. A Walsh-type diagram (Figure 15), in which the coupling between the imido groups is ignored, shows approximate MO energies based on DFT calculations for UN_2.[46] Initially, the $2p_z(\sigma)$ orbitals are ~1.5 eV *above* $2p_{x,y}(\pi)$ as a result of the small $U(5f_\sigma)-O(2p_\sigma)$ overlap and the "pushing from below" interaction with $U(6p_\sigma)$.[6,46,48] If a proton (or carbonium ion) is added axially, the $2p_z(\sigma)$ MO, as calculated by Boncella,[88] is ~2.5 eV *below* $2p_{x,y}(\pi)$ and is stabilized by ~4 eV. If the proton is then moved to the *x*-axis to give a U−N−H angle of 90°, the $2p_z$ MO returns to its original energy in UN_2, but the $2p_x$ MO is lowered by ~4 eV, this being the equivalent of the stabilization of $2p_z$ on protonation.

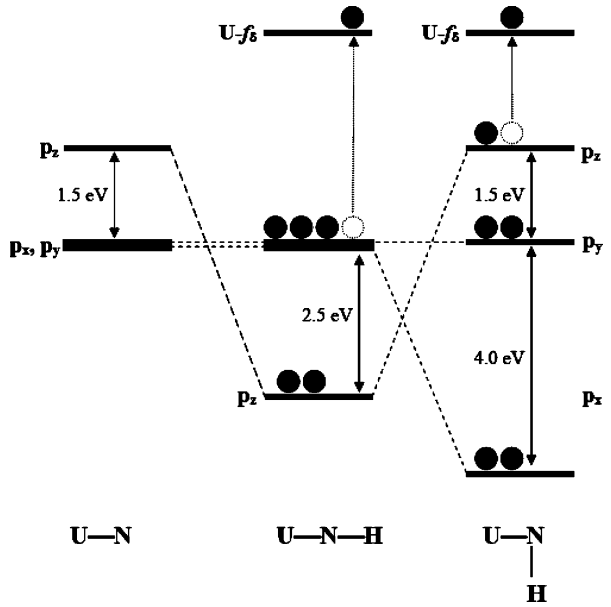

Figure 15. Walsh diagram for nitrido and imidouranium units.

In this simple model, the sum of the orbital energies in the electronic ground state is the same for both linear and bent geometries. However, in the first excited state, when one electron is promoted to the nonbonding $U(5f_\delta)$ (Figure 15), the bent geometry exhibits a relative stabilization of ~1.5 eV. This crude scheme ignores the decrease in U−N bond energy caused by the presence of the imido proton. The order of the bonding MOs in UN_2 suggests that this decrease should be largest in the bent geometry, because the π orbitals appear to have a stronger bonding interaction with uranium than the σ orbitals. This factor should reduce the tendency to bend.

Several strands of evidence support the hypothesis of a bent excited state.

(a) If the nonbonding $5f_\delta$ electron is ignored and only the σ-components of the U−N−R bonds are considered, the excited state electronic structure is analogous to that of the linear NH_2 radical. This exhibits a strong Renner−Teller instability and, at equilibrium, is stabilized by 1.48 eV at a H−N−H bond angle of 103.4°.[94]

(b) Computed ground state potential surfaces for M−N−R bending in transition metal−imido compounds are essentially flat.[95,96]

(c) Analogous optical excitations in the d^0 species $M(NR)Cl_3$(dimethylethanediol), where M = Nb or Ta are assigned to transitions from the M = N π-type bonding orbitals to a vacant d_{xy} orbital that is nonbonding with respect to the imido ligand.[97] The absorption and emission spectra of these compounds are broad and featureless at room temperature and show very large (~10 000 cm^{-1}) Stokes shifts.[97,98] In the solid state at 13 K, Ta(*N*-2,6-diisopropylphenyl)Br_3(tetramethylethylenediamine) shows a broad emission spectrum containing a poorly resolved 1100 cm^{-1} progression in the Ar−N stretching mode.[98] Evidently, the excited state is strongly distorted along the Ta−N coordinate, but this does not preclude a simultaneous distortion in the bending coordinate. Indeed, the broad emission spectrum suggests that the final states form part of a set of high spectral density, low-frequency, vibronic states, as expected for a soft bending potential.

TABLE 5: Bond Lengths and Vibrational Frequencies of Several MO_2^+ and MO_2^{2+} Species (Theoretical Values in Italics)

	UO_2^+		UO_2^{2+}		NpO_2^+		NpO_2^{2+}		
compound	R(U−O)/pm	ν_s, ν_{as}/cm^{-1}	R(U−O)/pm	ν_s, ν_{as}/cm^{-1}	R(U−O)/pm	ν_s, ν_{as}/cm^{-1}	R(U−O)/pm	ν_s, ν_{as}/cm^{-1}	ref
$MO_2(H_2O)_5^{+/2+}$	*181.0*	*840*, *909*	176.6 *175.6*	869, 965	185	767, 824	175 *175.2*	854, 969	42, 109−111
$MO_2(Ph_3PO)_4^{+/2+}$	182.1		176.2		179.2				104
MO_2(18-crown-6)$^{+/2+}$			163.5(50)		180.0	778			112
$MO_2(Py)_5^{+/2+}$	183.6	797							103, 105
$MO_2(Py)_3I_2$			175.5	927					113
MO_2(Saloph)(DMSO)$^{-1/0}$		770		895					114
$[NpO_2MoO_4(H_2O)]^{-1/0}$					185.4				102

(d) If the equilibrium configuration of the excited state is bent, then when the U−N−R angle is close to 180° the bending potential function must be almost flat. Vertical optical excitations will then occur to states that are highly vibronically excited with respect to low-frequency bending modes, but which are also very closely spaced. The bending instability can therefore account for the absence of resolved vibronic structure in absorption and emission.

(e) A scalar relativistic DFT calculation on the isolated UONH molecule finds bond lengths of U−O 170.9, U−N 176.0, and N−H 105.3 pm. Keeping these distances fixed, the total energy of an excited $\pi^3\phi$ configuration, in which a π-type hole in the HOMO is largely localized on the nitrogen atom, was investigated as a function of the U−N−H angle. A minimum is found at 151°, this geometry being 621 cm^{-1} more stable than the linear case.[99] A more realistic calculation seems justifiable.

IV.1.5. Implications. Following this argument, actinyl analogs containing only *monatomic* ligands such as carbon, nitrogen, oxygen, or a halogen should show the highly resolved optical spectra characteristic of excitations from a σ-type HOMO, but imido ligands and their isoelectronic analogs, in which the HOMO is of π-type symmetry, will inevitably have broad featureless spectra associated with bent excited states that will hinder a detailed analysis of excited state properties. In this context we note that the low-temperature absorption and emission spectra of $(PPh_4)UOCl_5$ do show well-resolved progressions in both the U−O and axial U−Cl stretching modes of the $UOCl^{3+}$ structural unit.[71] The Huang−Rhys factors in these progressions indicate that, in the excited state, the hole in the HOMO is predominantly centered on oxygen. The much higher frequency of the axial U−Cl stretch compared to the equatorial U−Cl stretch is an illustration of the ITI (section III.7).[8]

IV.2. Stable UO_2^+ Compounds. The NpO_2^+ ion is well-known,[100−102] but UO_2^+ compounds have been difficult to isolate and characterize. Although UO_2^+ disproportionates rapidly in water it has recently been isolated in the solid state as $UO_2(Py)_{2.2}I_2K$,[103] $UO_2I(THF)_{2.7}$,[103] and $UO_2(OTf)(THF)_{1.5-2}$[103] and has been structurally characterized in $[UO_2(OPPh_3)_4](OTf)$[104] and $[UO_2Py_5][KI_2Py_2]$.[103,105] In solution the equatorial five-coordinate species, $[UO_2(saloph)DMSO]^-$ and $[UO_2(dbm)_2DMSO]^-$, six-coordinate $[UO_2(CO_3)_3]^{5-}$, and several other complexes can be prepared by electrochemical reduction of UO_2^{2+}.[106,107] Their near IR optical spectra show characteristic weak f−f transitions, analogous to those of the isoelectronic ($5f^1$) neptunyl(VI) ion.[20] However, relatively intense transitions, assigned as $^2\Phi_{5/2} \rightarrow {}^2\Pi_{1/2}$ and $^2\Pi_{3/2}$, occur near 11 000 and 13 500 cm^{-1}. The corresponding transitions in $[NpO_2(NO_3)_3]^-$ are found near 17 800 and 20 800 cm^{-1}.[20] The implication is that, in the more ionic UO_2^+, the $5f_\pi^*$ orbitals are less antibonding than in NpO_2^{2+}. The actinyl $3\sigma_u \rightarrow 5f_{\delta,\phi}$ absorption threshold occurs above 25 000 cm^{-1} for UO_2^+,[106] whereas it is near 20 000 cm^{-1} in UO_2^{2+} and 14 000 cm^{-1} in NpO_2^{2+}.[108] These differences are consistent with the effective nuclear charge on the actinide atom.

Table 5 summarizes bond-length and vibrational data for some comparable MO_2^+ and MO_2^{2+} species.

IV.3. Unstable Species. *IV.3.1. Experimental Data.* In recent years laser ablation sources have led to the characterization of many new uranium species, both in inert gas matrices and in the gas phase. In particular, Andrews' group has studied the reaction of uranium atoms with N_2, CO, NO, O_2, and S_n in inert gas matrices. Among the triatomic products related to the uranyl ion that can be trapped are UO_2,[30,115−117] UO_2^+,[115,117−119] UO_2^-,[117] CUO,[116,120−123] UN_2,[124] UON,[125] UON^+,[125] and US_2.[126] All these species are linear with the exception of US_2, where an analysis of isotopic shifts finds that the S−U−S angle is 118 ± 5°. DFT calculations show that the overlap density in US_2 is dominated by 6d orbitals, and that the contribution to the bonding from the more contracted 5f set is quite small. The U−S distances are computed to be 238 pm[126] rather than the 170−190 pm typical of species containing first period atoms. In light of the radial amplitudes shown in Figure 10, the dominance of the 6d interaction at this distance is not surprising. In d^0 dioxo−transition metal analogs, where the d-shell dominates the bonding, bent geometry is the norm and is thus is not unexpected here.

Table 6 shows vibrational frequencies for the remainder of these triatomic species. In most cases these are the only observables, apart from the isotopic analyses that confirm the composition and linearity. The remainder of the data in the table is drawn from theoretical calculations. Several features deserve comment.

(a) In UO_2^{2+}, UO_2^+, and UO_2, the asymmetric stretching frequencies drop sharply from ∼1100 to 915 cm^{-1} with decreasing oxidation state, and the calculated U−O distances increase from ∼173 to 183 pm. The UO_2^{2+} species in the gas phase are mass-selected by ion-cyclotron resonance, and their IR spectra are measured using a free-electron laser.[127] In $UO_2^{2+}(acetone)_n$, with $n = 4$, 3, and 2, and $UO_2^{2+}(MeCN)_m$ with $m = 5$, 4, and 3, the O−U−O frequency rises progressively to ∼1020 cm^{-1} as the number of ligands decrease. This trend is fairly well modeled using the B3LYP exchange−correlation functional, provided that the resulting frequencies are empirically scaled by a factor of 0.975. Extrapolation to the bare UO_2^{2+} gaseous ion predicts a frequency of 1116 cm^{-1}.[127]

(b) In the U(VI) species UON^+ and CUO (in neon), the U−N and U−C stretching modes occur at higher frequency than the U−O stretch. After allowing for the mass of the oscillators the U−N and U−C bonds appear to have higher force constants than U−O and, according to theory, are between 3.5 and 5 pm shorter. The isoelectronic series UO_2^{2+}, UON^+, and CUO are formally derived by the stepwise removal of a proton from one of the oxo ligands in UO_2^{2+}, leading to a progressive rise in the energy of the N and C based valence orbitals relative to

TABLE 6: Experimental and Calculated (in Italics) Bond Data for Various Uranium Triatomic Species

OS	species	ν_{asym}	ν_{sym}	U−X/pm	U−O/pm	GS	ref
VI	$UO_2^{2+}O_2^{2-}$(in Ar)	952.3				$^1\Sigma^+$	115
	UO_2^{2+}(acetone)$_2$(g)	1017			*174.5*	$^1\Sigma^+$	127
	UO_2^{2+} (g)	1112−1140			*172.8*		
					171.6		46
	UON^+ (in Ar)	1017 (U−N)	868.4 (U−O)	*169.8*	*175.8*	$^1\Sigma^+$	125
				171.2	*176.7*		47
				165.9	*175.1*		46
	UN_2 (in Ar)	1051/*1123*	1008.3 (*1087*)	*171.7*		$^1\Sigma^+$	124, 128
				173.4			46
	$CUO(Ne)_4$	1047.3 (U−C)	872.2 (U−O)	*176.9*	*180.5*	$^1\Sigma^+$	116
		983	*847*				
	$CUO(Ar)_4$	852.5 (U−C)	804.3 (U−O)	*187.1*	*183.3*	$^3\Phi$	116
		869	*814*				
V	UON (in Ar)	983.6 (U−N)	818.9 (U−O)	*175.7*	*183.7*	$^2\Phi$	125
		1005	*846*				
	$UO_2(Ne)_6^+$	980.1/*985*			*177.6*	$^2\Phi_u$	119
IV	UO_2 (in Ne)	914.8/*919*			*183.5*	$^3\Phi_u$	117, 118
	UO_2 (in Ar)	776/*805*			*190.1*	^3H_g	115, 118

those on uranium. As a result, these bonds become increasingly covalent; they are shorter than U−O and dominate the interactions with uranium. The reduced charge on uranium leads to an increase in the U−O distance from ∼173 pm in UO_2^{2+} to 176 pm in UON^+ and 180 pm in CUO.

(c) There are unexpected changes in the electronic ground states. If CUO is isolated in an argon matrix, rather than a neon matrix, the C−U frequency changes from 1047 to 852.5 cm^{-1} and the U−O mode changes from 872.2 to 804.3 cm^{-1}. These effects greatly exceed the matrix induced shifts found in other species and are taken to indicate the presence of weak bonding interactions between argon and uranium. A variety of calculations, the best of which incorporate the spin−orbit interaction, suggest that two states, $^1\Sigma^+_0$ and $^3\Phi_2$, have very similar energies.[116,120−123,129,130] Their conclusions are strongly dependent on the detailed procedures for handling electron correlation.[130] The singlet corresponds to the familiar closed-shell actinyl-like configuration in which all electrons occupy bonding orbitals, and the triplet is obtained by a notional excitation from the HOMO to a $5f_\phi$ orbital.[129] The small energy difference between these orbitals is due to the low electronegativity of carbon and the nonbonding nature of $5f_\phi$. Because the main ligand contribution to the HOMO is from $C(2p_\sigma)$, in the $^3\Phi_2$ state the C−U frequency drops by 195 cm^{-1} whereas the U−O mode drops by only 68 cm^{-1}. Andrews' calculations show that the binding energy of an argon atom in $CUO(Ar)_4$ is 6.8 kJ/mol, exceeding that of a neon atom by 2.0 kJ/mol.[116] These results need to be treated with caution because it is known that DFT functionals perform poorly in describing long-range charge-transfer interactions.[131] The stronger Ar binding leads to a reduction of the nominal positive charge (to +1.35) on uranium,[116] so a significant factor in stabilizing the triplet state will be the reduced electron−electron repulsion associated with the concomitant expansion of the $5f_\phi$ orbitals.

(d) The UO_2 molecule in an inert gas matrix formally contains uranium(IV) and, in common with other U(IV) compounds, might be expected to have a $5f^2$ ground state configuration. Due to the upward shift in the uranium-centered atomic orbital energies compared to UO_2^{2+}, a more ionic U−O bond is expected. Remarkably, very different O−U−O stretching frequencies are found in argon (776 cm^{-1}) and neon (914.8 cm^{-1}) matrices.[118] Apparently, two electronic states with very different bonding characters have similar energies. Calculations suggest that a $^3H_{4g}$ state, stemming from the $5f^2(\delta\phi)$ configuration, is the ground state in argon, but that a $^3\Phi_{2u}$ state from the $5f^17s^1$ configuration is the ground state in neon.[118] The latter configuration is destabilized in the presence of the stronger equatorial argon ligands, due to the relatively large antibonding interactions of these ligands with 7s. Indeed, the equilibrium U−Ar distance in the $^3\Phi_{2u}$ state is calculated to be almost 100 pm longer than that in the $^3H_{4g}$ state. In line with the observed frequencies, scalar-relativistic DFT and CCSD(T) calculations indicate that the U−O bond length (180.8 or 183.3 pm) in the $^3\Phi_{2u}$ state is 5−7 pm shorter than that in the $^3H_{4g}$ state (185.6 or 190.1 pm). This is not easy to explain using a simple valence model because in the $^3H_{4g}$ ($5f^2(\delta\phi)$) state both electrons are nonbonding toward oxygen, whereas in the $^3\Phi_{2u}$ ($5f^17s^1$) state one occupies the 7s orbital that is nominally antibonding toward oxygen. On the other hand, the extreme diffuseness of 7s (Figure 10) leads to both a very small overlap with O(2p) (cf. Table 3) and reduced repulsion toward oxygen-centered density, in contrast to the $5f^2$ configuration where the second electron occupies the more contracted 5f shell.

The absorption spectrum of UO_2 in the gas phase, cooled in a supersonic nozzle expansion, has been measured using resonance-enhanced multiphoton ionization detection.[132] It can be analyzed in terms of 7s → 7p excitations from two closely spaced components, $^3\Phi_{2u}$ and $^3\Phi_{3u}$, derived from the $5f^17s^1$ configuration. The latter is found 350 cm^{-1} above the former. These results are well modeled by a CASPT2-RASSI calculation,[133] which finds these states to be separated by 378 cm^{-1} and predicts the presence of excited states from the $5f^17p^1$ configuration that approximately match the energy of the intense absorption bands in the visible. Significantly, the $^3H_{4g}$ $5f^2(\delta\phi)$ state is calculated to lie 3330 cm^{-1} above the $^3\Phi_{2u}$ ground state. However, transitions to $5f^2$ states are predicted to have negligible intensity, and there is no evidence for these states in the spectrum.

Heaven's group have also studied the fluorescence and fluorescence excitation spectra of UO_2 in an argon matrix.[134] The consistency between these spectra and those in the gas phase suggest that the ground state has *ungerade* symmetry and is the same in both phases. This conflicts with the interpretation of the low stretching frequency observed in an argon matrix by Andrews, which appears to indicate a *gerade* $^3H_4$ $5f^2(\delta\phi)$ ground state.[117,118] The incompatibility between these two sets of results is as yet unresolved.

IV.3.2. Summary. The unstable U(VI) species in Table 6 retain the linear geometry, short bonds, and high vibrational frequencies of the typical actinyl group. This is also true of the reduced species UON and UO_2^+. However, there are also species that have strikingly different electronic structures. The ground state

of CUO in a neon matrix has the familiar closed shell actinyl configuration, in which the HOMO has predominantly carbon $2p_\sigma$ character. However, in the more coordinating argon matrix an electron is transferred from this orbital to a uranium $5f_\phi$ orbital to give a $^3\Phi$ ground state. This is made possible by the low electronegativity of carbon (relative to oxygen), and reduced electron−electron repulsion in the $\sigma\phi$ configuration. The removal of an electron from the carbon-centered HOMO weakens the U−C bond much more than the U−O bond.

The other striking case is UO_2. Regardless of the unresolved ambiguity concerning the ground state, it is clear that the ^3H_g ($5f^2$) and $^3\Phi_u(5f7s)$ states have similar energies. The latter appears to be the ground state in the gas phase. At first sight this configuration is surprising because UO_2 is a more ionic species than UO_2^{2+} and could be compared to the paramagnetic phase of bulk UO_2 whose electronic excitations are characteristic of a $5f^2$ configuration in a cubic crystal field.[135] However, the 185 pm U−O distance calculated[118] for gas-phase UO_2 is much shorter than the 236.3 pm distance in the bulk UO_2 fluorite structure.[136] In the solid dioxide the Madelung potential of eight oxide neighbors enhances the ionic character, ensuring a higher effective positive charge on uranium. The distance in gas-phase UO_2, however, is typical of the strong short actinyl bonds, whose covalency explains the low calculated Mulliken charge on uranium of +1.26.[117] Although the gaseous ions U^{3+}, U^{4+}, and U^{5+} are calculated to have $5f^n$ ground state configurations, the neutral atom ground state configuration is $5f^36d7s^2$, and that of the U^+ is $5f^37s^2$, so the stability of a 5f7s ground state in UO_2 is consistent with the low positive charge on uranium.[60] Clearly the omission of the 7s orbital from the active valence shells adopted in section I (Figure 1) cannot be justified for actinyl analogs in which the uranium is in a low formal oxidation state.

V. Actinyl-Like Geometry

Whereas UF_6 and UCl_6 have a regular octahedral geometry, the isoelectronic UO_6^{6-} unit is, in the great majority of cases, distorted and better described as a uranyl oxide complex anion $(UO_2)O_4^{6-}$. Pyykko has highlighted this difference and investigated it computationally.[137] Here we argue that it is due to the more ionic character of UF_6, which militates against the adoption of the short covalent multiple bonds characteristic of actinyl ions.

The U−F distance in UF_6 is 199.9 pm. However, the U−F distances in the unknown gaseous ions FUF^{4+}, OUF^{3+}, NUF^{2+}, and CUF^+, all of which are isoelectronic with UO_2^{2+}, have been calculated to be 174.3, 179.2, 188.5, and 203.7 pm, respectively.[137] Evidently a decrease in the electronegativity of the atom trans to fluorine reduces the positive charge on uranium, making the U−F bond relatively ionic and comparable to, or longer than, that in UF_6 Similarly, in the organo-imido complex $[(Me_3Si)_2N]_3U(NSiMe_3)F$, the U−F bond is trans to the short (185.4 pm) covalent U−imido bond (cf. section IV.1.1) and is itself long at 201.3 pm.[83] This bond should be relatively ionic due to the strong donation from the three amido ligands, and this lengthens and weakens these bonds.

In Pyykko's comparison of UF_6 and the isolated UO_6^{6-} ion,[137] the latter is found to have an octahedral equilibrium geometry. However, it is also predicted to have a soft $e_g(2z^2-x^2-y^2)$ stretching deformation, one limit of which corresponds to the axially compressed actinyl geometry found in numerous uranates(VI),[137,138] e.g., $BaUO_4$.[139] In three cases uranium occupies a regular octahedral site with bond lengths very close to the value of 208.2(4) pm found in cubic δ-UO_3.[140] Note, however, that δ-UO_3 is ~10 kJ mol^{-1} less stable that the more dense γ-phase, in which a distorted octahedral uranium site exhibits the short (179 pm) uranyl grouping.[141]

The remaining oxide structures fall into two groups. The larger of these exhibits axial compression toward actinyl geometry, with axial and equatorial bond lengths clustering near 190 and 220 pm, respectively. In the smaller group there is axial elongation with distances near 230 and 200 pm. A plot of the axial versus equatorial distance is approximately linear with a slope of −1.74, close to the factor of −2 expected in an $e_g(2z^2-x^2-y^2)$ stretching mode. Pyykko's calculations show no equivalent softness in this mode in UF_6,[137] so the actinyl distortion must be favored by the greater covalency of the hexaaoxo ion.

Though no explicit orbital analysis has yet been undertaken, it is possible to attribute the tendency to distort to the larger extension of the 6d orbitals compared to the more tightly bound 5f (Figure 10). The sensitivity of the 5f orbital overlap to U−O bond length is made clear by the electronic structural data in section I. For example, these orbitals, enhanced by 6p hybridization, make a large contribution to the axial U−O bonding interactions at ~175 pm, but the equatorial field parameters[8] indicate that they interact only weakly (~0.2 eV) with equatorial oxygen ligands at greater distances, such as the 248 pm distance found in $RbUO_2NO_3$.[10,67] At the intermediate U−O distance of 208 pm found in octahedral sites, the manifold of filled orbital energies should resemble those in UF_6 (where U−F 199.9 pm), although the increased covalency should increase their energy span.

Orbital energies in UF_6, obtained from photoelectron spectroscopy[142] using Koopman's approximation, agree well with both scalar[143] and fully relativistic calculations.[144,145] They are shown in Figure 16. Straka et al.[143] offer a simplified interpretation of the bonding. The t_{1g} orbital is nonbonding by symmetry and acts as a reference level. The $1t_{1u}$ and $2t_{1u}$ orbitals lie respectively 1.4 eV below and 1.2 eV above this level and, taken together, do not make a significant contribution to the bond. The remaining bonding orbitals t_{2g}, e_g, a_{1g}, and t_{2u} accommodate 18 electrons, to give a nominal U−F bond order of 1.5.[143] However, in Figure 16 the t_{2g} and e_g ligand combinations, which interact with 6d, are substantially more strongly bonding than either a_{1g} or t_{2u}, which interact with 7s and 5f(π), respectively.

Turning to the axially compressed actinyl geometry, we now assume that all 5f interactions with ligands in the equatorial plane are negligible at ~230 pm. On the other hand, the short 175 pm axial U−O distances enable the formation of six strong bonds using both 5f ($\sigma + 2\pi$) and 6d ($\sigma + 2\pi$). In the equatorial plane the diffuse $6d_{x^2-y^2}$ and $6d_{xy}$ orbitals lead to σ and π bonds with the b_{1g} and b_{2g} ligand combinations, respectively (Figure 16). Table 4 shows that in $Cs_2UO_2Cl_4$ the 6d interactions with equatorial chlorides are still significant at 267 pm, so these should also be important for uranates with four oxide ions at ~230 pm.

The net effect, then, of an axially compressed distortion, is to replace the 5 ($2\sigma + 3\pi$) medium strength 6d bonding interactions of the octahedron, with 3 ($\sigma + 2\pi$) short axial bonds that are strong and 2 equatorial bonds that are weak, and to replace 3 weak (t_{2u}) 5f(π) orbital interactions with three ($\sigma + 2\pi$) strong axial interactions, the former being enhanced by the role of $6p_\sigma$. This is illustrated schematically in Figure 16, where major changes due to the strong axial interactions are indicated by thick links to octahedral parents and the smaller changes associated with the lengthened equatorial interactions are represented by thin lines. The orbital ordering at the tetragonal

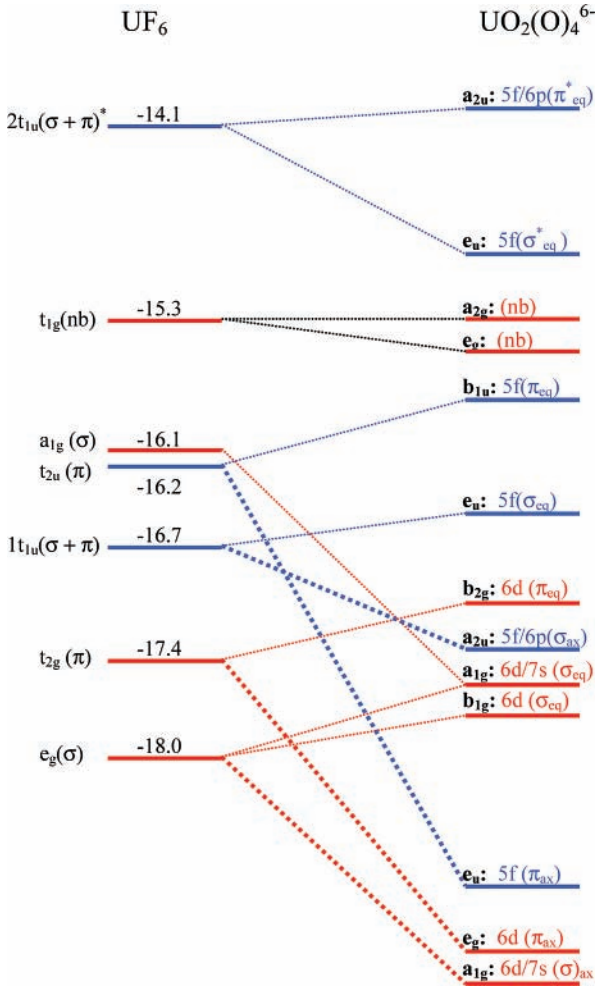

Figure 16. Evolution of octahedral valence orbital energies into tetragonal actinyl geometry: *gerade* orbitals, red; *ungerade* orbitals, blue.

limit is modeled on that computed for $Cs_2UO_2Cl_4$ (see Table 4). Put another way, there may be little change overall in the extent of 6d bonding but, because of the contracted nature of the 5f orbitals and their potential mixing with 6p, more is gained by shortening the axial bonds than is lost by lengthening those in the equatorial plane.

This description is entirely qualitative, but the question posed by Pyykko remains important. In the DFT era orbital-based analyses are uncommon but if this picture can be validated theoretically it would provide a useful guide to the origin of the ubiquitous presence of actinyl-like groups.

VI. Conclusions

The principal conclusions of the previous review[8] remain valid. They can, however, now be reinforced by new experimental data and more sophisticated theoretical work. The main features are as follows:

(1) The characteristics of the actinyl structural unit can now be seen to be shared by an extended class of compounds and a variety of oxidation states. These include CUO, OUN^+, $[R-N{=}U{=}N-R]^+$, arguably $UOCl^{3+}$ (in $[UOCl_5]^-$) and UO_2(g), as well as the well-known dioxo cations, AnO_2^{n+}. Because US_2 is bent, the short strong bonds of these triatomic units appear to be confined to first short period ligands, although Pyykko has recently calculated that linear species of the type OUM (M = Ir, Pt, Au^+) ought to exist in the gas phase.[146]

(2) The first excited states of the uranyl ion and its isoelectronic analogs are well described by excitations from a σ_u orbital to $5f_\delta$ and $5f_\phi$. Complete active space calculations that take account of the spin−orbit interaction are capable of a remarkably accurate description of the energies, vibrational frequencies, and bond lengths of these states, in a realistic equatorial ligand environment.

(3) Although DFT calculations indicate that the highest occupied molecular orbitals are usually centered on the equatorial ligands, the lowest energy excitations can nevertheless be viewed as effectively confined to the orbitals of the linear actinyl unit.

(4) A combination of spectroscopic and computational work makes it possible to construct an experimental orbital energy level diagram for the UO_2^{2+} ion that includes all the significant valence orbitals, be they filled or vacant.

(5) On the evidence available, the $6p_\sigma/5f_\sigma$ hybrids, in which An−O overlap is enhanced by the 6p component, make a large contribution to the bond, as does $6d_\pi$ whose overlap integrals are large. There are, however, subtle aspects to the other two components of the bond. Excitations from the nonbonding $5f_{\delta,\phi}$ to the $5f_\pi^*$ orbitals in the neptunyl ion cause only a small (4.9 pm) increase in the Np−O bond length (section II.1.4), indicating that the $5f_\pi^*(3\pi_u)$ are weakly antibonding, whereas in the uranyl ion an excitation from their bonding counterparts, $2\pi_u$, to the nonbonding $5f_{\delta,\phi}(1\delta_u$ or $1\phi_u)$ is predicted to lead to an increase of 18.6 pm (section III.3.2). Similarly, although the diffuse $6d_\sigma^*$ orbital appears to participate only weakly due to its small overlap (Table 1 and section II.3), an excitation from its bonding counterpart, $3\sigma_g$, to $1\delta_u$ increases the U−O bond length by 18 pm (section II.1.4).

(6) It is significant that those excitations that correspond to large oxygen to actinide charge transfer (from $3\sigma_g$ or $2\pi_u$ to $1\delta_u$) cause major increases in bond length, whereas those which are more uranium centered (i.e., from $3\sigma_u$ to $1\delta_u$, or from $1\delta_u$ to $3\pi_u^*$) have a much smaller effect. The expectation of a symmetrical relationship between bonding and antibonding interactions assumes a frozen orbital approximation and can be misleading. An oxygen to uranium charge-transfer excitation from the bonding orbitals (e.g., $2\pi_u$) of UO_2^{2+} to the nonbonding uranium $5f_{\delta/\phi}$ redistributes charge in the excited state in such a way as to lower the energies of all oxygen based MOs and raise those on uranium. It should therefore decrease the covalent bonding interactions in all the valence orbitals, not just that from which the excitation has taken place, and thus reinforces the bond weakening. On the other hand, the $5f_{\delta/\phi} \rightarrow 5f_\pi^*(3\pi_u^*)$ excitation in the NpO_2^{2+} ion shifts charge toward oxygen. Although the $3\pi_u^*$ electron is antibonding, the charge redistribution should strengthen the bonding valence interactions, so that the net change in bond length is relatively small. This interpretation is suggestive but needs theoretical substantiation.

(7) The low-intensity, highly resolved, vibronic structure observed in the optical spectrum of actinyl-like units containing monatomic ligands appears to be uniquely associated with excitations from a σ-symmetry valence orbital. Polyatomic analogs, on the other hand, as found in the newly characterized An=N−R imido species, lead to a reordering of the filled MOs, so that the lowest energy excitations occur from orbitals of π-symmetry. In these cases the electronic spectra are invariably broad and featureless. There is some evidence that this indicates the presence of an excited state Renner−Teller instability with respect to a bent U−X−Y geometry.

(8) The An−imido species are more covalent that their dioxo analogs and as a result show evidence of a preference for soft π-acceptor ligands.

(9) The main features of actinyl-like electronic structure are maintained across a broad range of compounds. However, substantial modifications occur, either when the charge on uranium becomes sufficiently small, as in UO_2, or when the electronegativity of one of the ligands is small, as in CUO.

(10) It is suggested that the adoption, in oxide systems, of the triatomic actinyl-like structure as opposed to the regular octahedral geometry found in UF_6, is a consequence of additional bonding contributions from the 5f shell which, due to the contracted nature of this shell, are only substantial at the short distances found in these species. This hypothesis needs computational support.

Acknowledgment. I am most grateful for discussion and collaboration with, and assistance from, the following: Professor R. M. Pitzer, Dr. N. Kaltsoyannis, Professor J. C. Green, Professor L. Braicovich and his group at INFM Milano, and Dr. N. B. Brookes (ESRF).

Note Added after ASAP Publication. This Feature Article was published on Articles ASAP on April 27, 2007. Figures 10 and 14 were misprinted. The corrected version was published ASAP on May 8, 2007.

References and Notes

(1) Gibson, J. K.; Haire, R. G.; Santos, M.; Marcalo, J.; de Matos, A. P. *J. Phys. Chem. A* **2005**, *109*, 2768−2781.

(2) Lias, S. G.; Liebman, J. F.; Levin, R. D.; Kafafi, S. A. *NIST Standard Reference Database, Positive Ion Energetics, Version 2.01*, 1994.

(3) Blaise, J.; Wyart, J.-F. *Energy Levels and Atomic Spectra of Actinides*; CNRS: Paris, 1992; Vol. 20.

(4) Pepper, M.; Bursten, B. E. *Chem. Rev.* **1991**, *91*, 719−741.

(5) Schreckenbach, G.; Hay, P. J.; Martin, R. L. *J. Comput. Chem.* **1999**, *20*, 70−90.

(6) Kaltsoyannis, N. *Chem. Soc. Rev.* **2003**, *32*, 9−16.

(7) Kaltsoyannis, N.; Hay, P. J.; Li, J.; Blaudeau, J. P.; Bursten, B. E. In *The Chemistry of the Actinide and Transactinide Elements*, 3rd ed.; Morrs, L. R., Edelstein, N. M., Fuger, J., Katz, J. J., Eds.; Springer: Dordrecht, The Netherlands, 2006; p Chapter 17.

(8) Denning, R. G. *Struct. Bonding* **1992**, *79*, 215−276.

(9) Veal, B. W.; Lam, D. J.; Carnall, W. T.; Hoekstra, H. R. *Phys. Rev. B* **1975**, *12*, 5651−5663.

(10) Barker, T. J.; Denning, R. G.; Thorne, J. R. G. *Inorg. Chem.* **1992**, *31*, 1344−1353.

(11) Denning, R. G.; Snellgrove, T. R.; Woodwark, D. R. *Mol. Phys.* **1976**, *32*, 419−442.

(12) Fonger, W. H.; Struck, C. W. *J. Chem. Phys.* **1974**, *60*, 1994−2002.

(13) Barker, T. J.; Denning, R. G.; Thorne, J. R. G. *Inorg. Chem.* **1987**, *26*, 1721−1732.

(14) Watkin, D. J.; Denning, R. G.; Prout, K. *Acta Crystallogr.* **1991**, *C47*, 2517.

(15) Henderson, B.; Imbusch, G. F. *Optical Spectroscopy of Inorganic Solids*; Oxford University Press: Oxford, U.K., 1989.

(16) Islam, A.; Ikeda, N.; Nozaki, K.; Ohno, T. *J. Chem. Phys.* **1998**, *109*, 4900−4910.

(17) Denning, R. G.; Snellgrove, T. R.; Woodwark, D. R. *Mol. Phys.* **1979**, *37*, 1109−1143.

(18) Norris, J. O. W. D. Phil. Thesis, Oxford University, 1980.

(19) Roberts, M.; Alcock, N. W. Personal Communication, 1980.

(20) Denning, R. G.; Norris, J. O. W.; Brown, D. *Mol. Phys.* **1982**, *46*, 287−323.

(21) Denning, R. G.; Morrison, I. D. *Chem. Phys. Lett.* **1991**, *180*, 101−104.

(22) Hill, R. J.; Kemp, T. J.; Allen, D. M.; Cox, A. *J. Chem. Soc., Faraday Trans. I* **1974**, *70*, 847−857.

(23) Teterin, Y. A.; Baev, A. S.; Mashirov, L. G.; Suglobov, D. N. *Dok. Akad. Nauk SSSR [Phys. Chem.]* **1984**, *227*, 131−136.

(24) Denning, R. G.; Green, J. C.; Hutchings, T. E.; Dallera, C.; Tagliaferri, A.; Giarda, K.; Brookes, N. B.; Braicovich, L. *J. Chem. Phys.* **2002**, *117*, 8008−8020.

(25) Degroot, F. M. F.; Grioni, M.; Fuggle, J. C.; Ghijsen, J.; Sawatzky, G. A.; Petersen, H. *Phys. Rev. B* **1989**, *40*, 5715−5723.

(26) De Jong, W. A.; Visscher, L.; Nieuwpoort, W. C. *J. Mol. Struct. (THEOCHEM)* **1999**, *458*, 41−52.

(27) Templeton, D. H.; Templeton, L. K. *Acta Crystallogr.* **1982**, *A38*, 62−67.

(28) Krause, M. O.; Oliver, J. H. *J. Phys. Chem. Ref. Data* **1979**, *8*, 329.

(29) Hudson, E. A.; Allen, P. G.; Terminello, L. J.; Denecke, M. A.; Reich, T. *Phys. Rev. B* **1996**, *54*, 156−165.

(30) Hay, P. J.; Wadt, W. R.; Kahn, L. R.; Raffenetti, R. C.; Phillips, D. H. *J. Chem. Phys.* **1979**, *71*, 1767−1779.

(31) Newman, J. B. *J. Chem. Phys.* **1965**, *43*, 1691−1694.

(32) Belford, R. L.; Belford, G. *J. Chem. Phys.* **1961**, *34*, 1330−1332.

(33) De Jong, W. A.; Harrison, R. J.; Nichols, J. A.; Dixon, D. A. *Theor. Chem. Acc.* **2001**, *107*, 22−26.

(34) Garcia-Hernandez, M.; Willnauer, C.; Kruger, S.; Moskaleva, L. V.; Rosch, N. *Inorg. Chem.* **2006**, *45*, 1356−1366.

(35) (a) In this context the first actinyl cyanide complex, $[UO_2(CN)_5]^{3-}$, has recently been structurally characterized.[35b] It has close to D_{5h} symmetry. The U−O bond length (177.3 pm) and asymmetric stretching frequency (911 cm^{-1}) are unexceptional. (b) Berthet, J. C.; Thuery, P.; Ephritikhine, M. *Chem. Commun.* **2007**, 604−606.

(36) Sonnenberg, J. L.; Hay, P. J.; Martin, R. L.; Bursten, B. E. *Inorg. Chem.* **2005**, *44*, 2255−2262.

(37) Schreckenbach, G.; Hay, P. J.; Martin, R. L. *Inorg. Chem.* **1998**, *37*, 4442−4451.

(38) Sonnenberg, J. L.; Hratchian, H. P.; Hay, P. J.; Martini, R. L.; Schlegel, H. B.; Bursten, B. E. *Abstr. Pap. Am. Chem. Soc.* **2005**, *229*, U1063−U1063.

(39) Clavaguera-Sarrio, C.; Vallet, V.; Maynau, D.; Marsden, C. J. *J. Chem. Phys.* **2004**, *121*, 5312−5321.

(40) Ingram, K. I. M.; Haller, L. J. L.; Kaltsoyannis, N. *Dalton Trans.* **2006**, 2403−2414.

(41) Shamov, G. A.; Schreckenbach, G. *J. Phys. Chem. A* **2005**, *109*, 10961−10974.

(42) Hay, P. J.; Martin, R. L.; Schreckenbach, G. *J. Phys. Chem. A* **2000**, *104*, 6259−6270.

(43) Buhl, M.; Kabrede, H. *Inorg. Chem.* **2006**, *45*, 3834−3836.

(44) Farkas, I.; Banyai, I.; Szabo, Z.; Wahlgren, U.; Grenthe, I. *Inorg. Chem.* **2000**, *39*, 799−805.

(45) Vallet, V.; Wahlgren, U.; Schimmelpfennig, B.; Szabo, Z.; Grenthe, I. *J. Am. Chem. Soc.* **2001**, *123*, 11999−12008.

(46) Kaltsoyannis, N. *Inorg. Chem.* **2000**, *39*, 6009−6017.

(47) Heinemann, C.; Schwarz, H. *Chem-Eur. J.* **1995**, *1*, 7−11.

(48) Dekock, R. L.; Baerends, E. J.; Boerrigter, P. M.; Snijders, J. G. *Chem. Phys. Lett.* **1984**, *105*, 308−316.

(49) Matsika, S.; Pitzer, R. M. *J. Phys. Chem. A* **2001**, *105*, 637−645.

(50) Matsika, S.; Zhang, Z.; Brozell, S. R.; Blaudeau, J. P.; Wang, Q.; Pitzer, R. M. *J. Phys. Chem. A* **2001**, *105*, 3825−3828.

(51) Zhang, Z. Y.; Pitzer, R. M. *J. Phys. Chem. A* **1999**, *103*, 6880−6886.

(52) Matsika, S.; Pitzer, R. M. *J. Phys. Chem. A* **2000**, *104*, 4064−4068.

(53) Pierloot, K.; van Besien, E. *J. Chem. Phys.* **2005**, *123*, 204309.

(54) Roos, B. O.; Lindh, R.; Malmqvist, P. A.; Veryazov, V.; Widmark, P. O. *Chem. Phys. Lett.* **2005**, *409*, 295−299.

(55) Andersson, K.; Malmqvist, P. A.; Roos, B. O. *J. Chem. Phys.* **1992**, *96*, 1218−1226.

(56) Roos, B. O.; Malmqvist, P. A. *Phys. Chem. Chem. Phys.* **2004**, *6*, 2919−2927.

(57) Pitzer, R. M. Private communication, quoted in ref 53.

(58) Szilagyi, R. K.; Metz, M.; Solomon, E. I. *J. Phys. Chem. A* **2002**, *106*, 2994−3007.

(59) Roothaan, C. C. J. *J. Chem. Phys.* **1951**, *23*, 69−89.

(60) Pyper, N. C.; Grant, I. P. *J. Chem. Soc., Faraday Trans. 2* **1978**, *74*, 1885−1900.

(61) Denning, R. G.; Ironside, C. N.; Snellgrove, T. R.; Thorne, J. R. G. *Mol. Phys.* **1982**, *47*, 443−456.

(62) Jorgensen, C. K. *Oxidation Numbers and Oxidation States*; Springer: Berlin, 1969; Chapter 7.

(63) Larsson, S.; Pyykko, P. *Chem. Phys.* **1986**, *101*, 355−369.

(64) Monard, J. A.; Huray, P. G.; Thomson, J. O. *Phys. Rev. B* **1974**, *9*, 2838−2845.

(65) Kalvius, G. M.; Dunlap, B. D.; Asch, L.; Weigel, F. *J. Solid State Chem.* **2005**, *178*, 545−553.

(66) Belanzoni, P.; Baerends, E. J.; Van Lenthe, E. *Mol. Phys.* **2005**, *103*, 775−787. This paper also includes a calculation on a "$[UO_2Rb(NO_3)_3]$ complex", having C_{3v} symmetry, in which a Rb^+ ion is bound axially to a single uranyl oxygen. Actually the space group of $RbUO_2(NO_3)_3$ is *R*3*c*, the uranium site symmetry is D_3 and both U−O bonds are identical.[67,68] The fictional C_{3v} structure has its origin in earlier work.[64]

(67) Barclay, G. A.; Sabine, T. M.; Taylor, J. C. *Acta Crystallogr.* **1965**, *19*, 205−209.

(68) Zalkin, A.; Templeton, L. K.; Templeton, D. H. *Acta Crystallogr., Sect. C* **1989**, *45*, 810−811.

(69) Joubert, P.; Weulersse, J. M.; Bougon, R.; Gaudreau, B. *Can. J. Chem.* **1978**, *56*, 2546−2549.

(70) Joubert, P.; Bougon, R.; Gaudreau, B. *Can. J. Chem.* **1978**, *56*, 1874−1880.

(71) Bartleet, J. M.; Denning, R. G.; Morrison, I. D. *Mol. Phys.* **1992**, *75*, 601−612.

(72) Bagnall, K. W.; Du Preez, J. G. H.; Gellatly, B. J.; Holloway, J. H. *J. Chem. Soc., Dalton Trans.* **1975**, 1963−1968.

(73) O'Grady, E.; Kaltsoyannis, N. *J. Chem. Soc., Dalton Trans.* **2002**, 1233−1239.

(74) Chermette, H.; Rachedi, K.; Volatron, F. *J. Mol. Struct. (THEOCHEM)* **2006**, *762*, 109−121.

(75) Kovacs, A.; Konings, R. J. M. *Chemphyschem* **2006**, *7*, 455−462.

(76) Dehnicke, K.; Strahle, J. *Polyhedron* **1989**, *8*, 707−726.

(77) Nugent, W. A.; Haymore, B. L. *Coord. Chem. Rev.* **1980**, *31*, 123−175.

(78) Green, M. L. H.; Hogarth, G.; Konidaris, P. C.; Mountford, P. *J. Chem. Soc., Dalton Trans.* **1990**, 3781−3787.

(79) Hogarth, G.; Konidaris, P. C. *J. Organomet. Chem.* **1990**, *399*, 149−152.

(80) Brennan, J. G.; Andersen, R. A. *J. Am. Chem. Soc.* **1985**, *107*, 514−516.

(81) Arney, D. S. J.; Burns, C. J. *J. Am. Chem. Soc.* **1993**, *115*, 9840−9841.

(82) Arney, D. S. J.; Burns, C. J.; Smith, D. C. *J. Am. Chem. Soc.* **1992**, *114*, 10068−10069.

(83) Burns, C. J.; Smith, W. H.; Huffman, J. C.; Sattelberger, A. P. *J. Am. Chem. Soc.* **1990**, *112*, 3237−3239.

(84) Brown, D.; Denning, R. G.; Jones, R. H. *J. Chem. Soc., Chem. Commun.* **1994**, 2601−2602.

(85) Brown, D. R.; Denning, R. G. *Inorg. Chem.* **1996**, *35*, 6158−6163.

(86) Williams, V. C.; Muller, M.; Leech, M. A.; Denning, R. G.; Green, M. L. H. *Inorg. Chem.* **2000**, *39*, 2538−2541.

(87) Hayton, T. W.; Boncella, J. M.; Scott, B. L.; Batista, E. R.; Hay, P. J. *J. Am. Chem. Soc.* **2006**, *128*, 10549−10559.

(88) Hayton, T. W.; Boncella, J. M.; Scott, B. L.; Palmer, P. D.; Batista, E. R.; Hay, P. J. *Science* **2005**, *310*, 1941−1943.

(89) Crawford, M. J.; Mayer, P. *Inorg. Chem.* **2005**, *44*, 5547−5549.

(90) Crawford, M. J.; Ellern, A.; Karaghiosoff, K.; Mayer, P.; Noth, H.; Suter, M. *Inorg. Chem.* **2004**, *43*, 7120−7126.

(91) Hayton, T. W.; Boncella, J. M.; Scott, B. L.; Batista, E. R. *J. Am. Chem. Soc.* **2006**, *128*, 12622−12623.

(92) Brown, D. R. D. Phil. Thesis, Oxford University, 1996, p 249.

(93) Williams, V. C. D. Phil. Thesis, University of Oxford, 1998, p 205.

(94) Gabriel, W.; Chambaud, G.; Rosmus, P.; Carter, S.; Handy, N. C. *Mol. Phys.* **1994**, *81*, 1445−1461.

(95) Cundari, T. R. *Chem. Rev.* **2000**, *100*, 807−818.

(96) Rankin, D. W. H.; Robertson, H. E.; Danopoulos, A. A.; Lyne, P. D.; Mingos, D. M. P.; Wilkinson, G. *J. Chem. Soc., Dalton Trans.* **1994**, 1563−1569.

(97) Williams, D. S.; Korolev, A. V. *Inorg. Chem.* **1998**, *37*, 3809−3819.

(98) Heinselman, K. S.; Hopkins, M. D. *J. Am. Chem. Soc.* **1995**, *117*, 12340−12341.

(99) Green, J. C. Personal Communication, 2006.

(100) Clark, D. L.; Keogh, D. W.; Palmer, P. D.; Scott, B. L.; Tait, C. D. *Angew. Chem. Int. Ed.* **1998**, *37*, 164−166.

(101) Grigor'ev, M. S.; Charushnikova, I. A.; Krot, N. N. *Radiochemistry* **2005**, *47*, 549−551.

(102) Grigor'ev, M. S.; Fedoseev, A. M.; Budantseva, N. A.; Antipin, M. Y. *Radiochemistry* **2005**, *47*, 545−548.

(103) Berthet, J. C.; Siffredi, G.; Thuery, P.; Ephritikhine, M. *Chem. Commun.* **2006**, 3184−3186.

(104) Berthet, J. C.; Nierlich, M.; Ephritikhine, M. *Angew. Chem. Int. Ed.* **2003**, *42*, 1952−1954.

(105) Natrajan, L.; Burdet, F.; Pecaut, J.; Mazzanti, M. *J. Am. Chem. Soc.* **2006**, *128*, 7152−7153.

(106) Mizuoka, K.; Tsushima, S.; Hasegawa, M.; Hoshi, T.; Ikeda, Y. *Inorg. Chem.* **2005**, *44*, 6211−6218.

(107) Shirasaki, K.; Yamamura, T.; Shiokawa, Y. *J. Alloy. Compd.* **2006**, *408*, 1296−1301.

(108) Denning, R. G.; Norris, J. O. W.; Brown, D. *Mol. Phys.* **1982**, *46*, 325−364.

(109) Neuefeind, J.; Soderholm, L.; Skanthakumar, S. *J. Phys. Chem. A* **2004**, *108*, 2733−2739.

(110) Combes, J. M.; Chisholmbrause, C. J.; Brown, G. E.; Parks, G. A.; Conradson, S. D.; Eller, P. G.; Triay, I. R.; Hobart, D. E.; Meijer, A. *Environ. Sci. Technol.* **1992**, *26*, 376−382.

(111) Madic, C.; Begun, G. M.; Hobart, D. E.; Hahn, R. L. *Inorg. Chem.* **1984**, *23*, 1914−1921.

(112) Deshayes, L.; Keller, N.; Lance, M.; Nierlich, M.; Vigner, J. D. *Acta Crystallogr., Sect. C* **1994**, *50*, 1541−1544.

(113) Berthet, J. C.; Nierlich, M.; Ephritikhine, M. *Chem. Commun.* **2004**, 870−871.

(114) Mizuoka, K.; Kim, S. Y.; Hasegawa, M.; Hoshi, T.; Uchiyama, G.; Ikeda, Y. *Inorg. Chem.* **2003**, *42*, 1031−1038.

(115) Hunt, R. D.; Andrews, L. *J. Chem. Phys.* **1993**, *98*, 3690−3696.

(116) Liang, B.; Andrews, L.; Li, J.; Bursten, B. E. *Inorg. Chem.* **2004**, *43*, 882−894.

(117) Zhou, M.; Andrews, L.; Ismail, N.; Marsden, C. J. *J. Phys. Chem. A* **2000**, *104*, 5495−5502.

(118) Li, J.; Bursten, B. E.; Andrews, L.; Marsden, C. J. *J. Am. Chem. Soc.* **2004**, *126*, 3424−3425.

(119) Wang, X.; Andrews, L.; Bursten, B. E. *Angew. Chem. Int. Ed.* **2004**, *43*, 2554−2557.

(120) Andrews, L.; Liang, B.; Li, J.; Bursten, B. E. *New J. Chem.* **2004**, *28*, 289−294.

(121) Li, J.; Bursten, B. E.; Liang, B.; Andrews, L. *Science* **2002**, *295*, 2242−2245.

(122) Liang, B.; Andrews, L.; Li, J.; Bursten, B. E. *Chem.−Eur. J.* **2003**, *9*, 4781−4788.

(123) Zhou, M.; Andrews, L.; Li, J.; Bursten, B. E. *J. Am. Chem. Soc.* **1999**, *121*, 9712−9721.

(124) Kushto, G. P.; Souter, P. F.; Andrews, L. *J. Chem. Phys.* **1998**, *108*, 7121−7130.

(125) Kushto, G. P.; Souter, P. F.; Andrews, L.; Neurock, M. *J. Chem. Phys.* **1997**, *106*, 5894−5903.

(126) Liang, B.; Andrews, L.; Ismail, N.; Marsden, C. J. *Inorg. Chem.* **2002**, *41*, 2811−2813.

(127) Groenewold, G. S.; Gianotto, A. K.; Cossel, K. C.; Van Stipdonk, M. J.; Moore, D. T.; Polfer, N.; Oomens, J.; de Jong, W. A.; Visscher, L. *J. Am. Chem. Soc.* **2006**, *128*, 4802−4813.

(128) Hunt, R. D.; Yustein, J. T.; Andrews, L. *J. Chem. Phys.* **1993**, *98*, 6070.

(129) Roos, B. O.; Widmark, P. O.; Gagliardi, L. *Faraday Discuss.* **2003**, *124*, 57−62.

(130) Infante, I.; Visscher, L. *J. Chem. Phys.* **2004**, *121*, 5783−5788.

(131) Ruiz, E.; Salahub, D. R.; Vela, A. *J. Am. Chem. Soc.* **1995**, *117*, 1141−1142.

(132) Han, J. D.; Goncharov, V.; Kaledin, L. A.; Komissarov, A. V.; Heaven, M. C. *J. Chem. Phys.* **2004**, *120*, 5155−5163.

(133) Gagliardi, L.; Heaven, M. C.; Krogh, J. W.; Roos, B. O. *J. Am. Chem. Soc.* **2005**, *127*, 86−91.

(134) Lue, C. J.; Jin, J.; Ortiz, M. J.; Rienstra-Kiracofe, J. C.; Heaven, M. C. *J. Am. Chem. Soc.* **2004**, *126*, 1812−1815.

(135) Amoretti, G.; Blaise, A.; Caciuffo, R.; Fournier, J. M.; Hutchings, M. T.; Osborn, R.; Taylor, A. D. *Phys. Rev. B* **1989**, *40*, 1856−1870.

(136) Slowinski, E.; Elliott, N. *Acta Crystallogr.* **1952**, *5*, 768−770.

(137) Pyykko, P.; Li, J.; Runeberg, N. *J. Phys. Chem.* **1994**, *98*, 4809−4813.

(138) King, R. B. *Chem. Mater.* **2002**, *14*, 3628−3635.

(139) Reis, A. H.; Hoekstra, H. R.; Gebert, E.; Peterson, S. W. *J. Inorg. Nucl. Chem.* **1976**, *38*, 1481−1485.

(140) Weller, M. T.; Dickens, P. G.; Penny, D. J. *Polyhedron* **1988**, *7*, 243−244.

(141) Siegel, S.; Hoekstra, H. R. *Inorg. Nucl.Chem. Lett.* **1971**, *7*, 455-&.

(142) Martensson, N.; Malmquist, P. A.; Svensson, S.; Johansson, B. *J. Chem. Phys.* **1984**, *80*, 5458−5464.

(143) Straka, M.; Patzschke, M.; Pyykko, P. *Theor. Chem. Acc.* **2003**, *109*, 332−340.

(144) Peralta, J. E.; Batista, E. R.; Scuseria, G. E.; Martin, R. L. *J. Chem. Theory Comput.* **2005**, *1*, 612−616.

(145) DeJong, W. A.; Nieuwpoort, W. C. *Int. J. Quantum Chem.* **1996**, *58*, 203−216.

(146) Hrobarik, P.; Straka, M.; Pyykko, P. *Chem. Phys. Lett.* **2006**, *431*, 6−12.